Ice Thickening Climate Repair

Katherine Cartlidge

The College of the Blessed Virgin Mary, Saint John the Evangelist
and the glorious Virgin Saint Radegund, near Cambridge

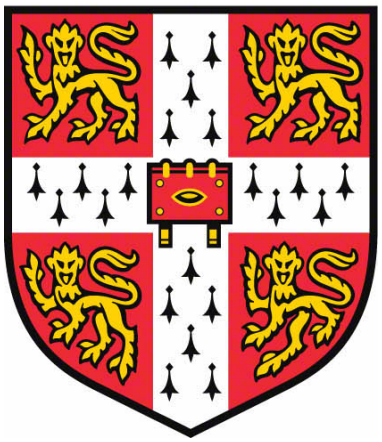

Department of Engineering
University of Cambridge
June 2022

Technical Abstract

We investigate the use of geoengineering to restore Arctic sea ice, by evaluating a proposal known as the 'ice volcano'. Seawater is pumped through a slotted pipe over a floating conical buoy, where it freezes in the cold Arctic atmosphere to generate a growing cone of ice. Once 3 metres of height has been achieved, the newly-formed ice is likely to survive a summer melting season and become valuable 'multi-year ice'. The presence of Arctic sea ice has numerous benefits, such as: inhibiting methane release from permafrost melt; increasing the proportion of incoming solar radiation that is reflected; maintaining global currents that mediate weather patterns in the Northern hemisphere; and providing a habitat for polar wildlife. Ice loss is of global relevance, since it forms part of a feedback loop that accelerates the rate of climate change. Its summer extent has decreased by more than 50% in the last 50 years and an ice-less September could be seen within the next decade. It is therefore of critical importance to restore Arctic sea ice.

Building on the work of Daniel Siromani and Herbert Huppert, we evaluate the feasibility of an ice volcano using a simplified, two-dimensional model. We begin with a theoretical analysis of the problem from first principles, for two fundamental cases: fresh water initially at its freezing temperature and fresh water initially above its freezing temperature. We find that, in the first case, the release of latent heat (from solidification of the water) must balance the conductive heat flux in the ice at the ice-water interface. In the second case, the latent heat must balance the difference between this conductive heat flux and a second, convective heat flux from the water to the ice. By considering behaviour at the instant the water touches the ice, we find that the interface between the two must be at the phase change temperature, and also that the first response of the system must be freezing at a very fast rate. This is due to the abrupt change in temperature profile of the solid, which tends towards the step function. These results are true irrespective of the original water temperature. For fresh water initially at its freezing temperature, it is shown that ice build-up is uniform along the channel and at a rate proportional to $1/\sqrt{t}$. For fresh water initially above its freezing temperature, the first response is always freezing, as above, followed by melting that occurs soonest at the channel inlet. Melting begins with the newly-formed ice. After some time, the expected ice profile is net ice loss near the inlet and net ice gain far from the inlet. This has mixed implications for the ice volcano, suggesting that the region of ice around the slotted pipe could be eroded.

This is followed by experimental analysis, using a narrow channel that maps onto the two-dimensional model. Experiments were conducted in a walk-in freezer of temperature –18°C. Water, of varying temperatures and salinities, was pumped through the channel over a layer of cold 'original ice' and allowed to freeze or cause melting, and the resulting change in ice thickness calculated. It was found that the ice profile is described well by the theoretical model for water above its freezing temperature, but the model underestimates ice growth for water at its freezing temperature. We propose that this is mainly due to the model neglecting heat transfer to the atmosphere and to the side walls of the channel. This is because this heat transfer becomes significant compared to conduction in the ice over the timescales of the experiments, but is still insignificant compared to convection from the water to the ice. This convection only occurs for water warmer than its freezing temperature.

Fresh water and water at 32 psu (the salinity of Arctic seawater) was used in the experiments. The 'ice' grown from salt water appeared in fact to be a two-phase mixture of fresh ice and

concentrated brine. Some of this brine was trapped in the ice matrix and some seemed to have been rejected into the bulk flow. More brine appeared to become trapped for water initially at its freezing temperature – this is an example of a 'mushy layer'. A useful outcome of the rejected brine is that the melting temperature of the salty ice is warmer than the freezing temperature of the original salt water. This means that, compared to fresh water equivalently warmer than its freezing temperature, less ice is eroded at the channel inlet, and that there is a wider temperature range over which an ice volcano could be feasible. This was also shown experimentally and is an encouraging result.

The theoretical analysis was based on fresh water, which has equal melting and freezing temperatures. Salt water experimental results were plotted alongside two theoretical predictions: one with the freezing temperature in the mathematical model set to –1.8°C, governing the freezing of the water; and one with the freezing temperature set to 0°C, governing the melting of the ice. These formed upper and lower bounds for the salt water results. Early in the experiment, and far from the channel inlet, the first prediction was a better fit, confirming that freezing was the dominant behaviour. Later in the experiment, and near the channel inlet, the second prediction was favourable, indicating the melting was the dominant behaviour.

The main insight from the theoretical and experimental analysis is that water entering above the melting temperature of the ice will cause catastrophic ice loss near the inlet, which must be avoided for an ice volcano to be feasible. We conclude with suggestions for how this issue could be prevented, and recommendations for further work on this topic.

Contents

1 Introduction

In April 1909, Robert Peary claimed to be the first person to set foot on the North Pole. His expedition comprised 26 men and 140 dogs, taking 5 weeks to traverse the frozen Arctic Ocean. However, that journey could soon be considerably faster: Arctic sea ice is declining so quickly that, at current rates, the North Pole will be accessible by boat within the next decade, and future explorers may not be able to 'set foot' on the pole at all. But aside from providing explorers with ground upon which to place their flags, polar ice has extraordinary importance, especially for the global climate. Its loss forms part of a feedback loop that accelerates global warming, eliciting the motivation for this project: regeneration of sea ice is critical in tackling climate change. The objective of this project is therefore to investigate geoengineering as a means to combat the loss of Arctic sea ice.

1.1 An introduction to Arctic sea ice

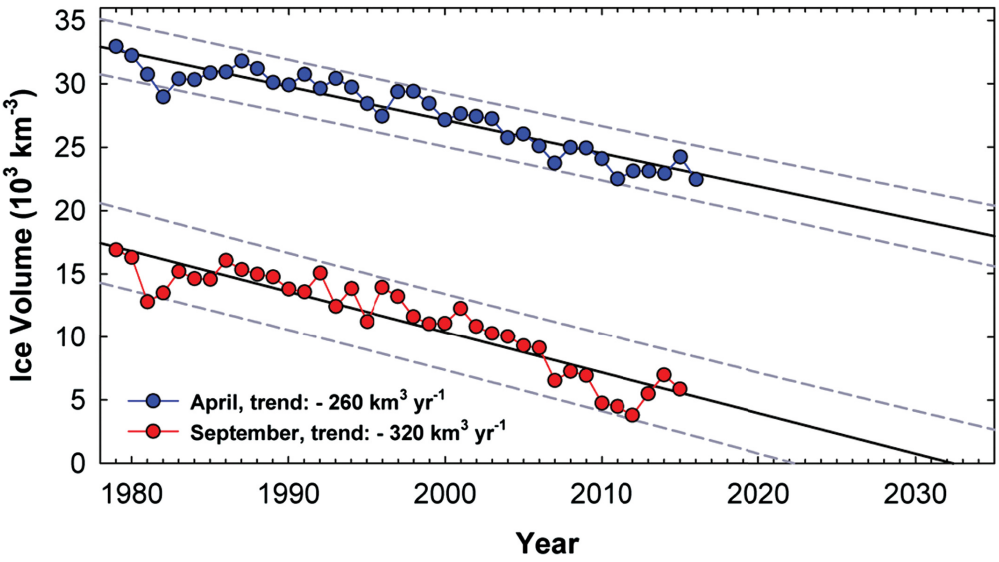

Figure 1: Volume of Arctic sea ice in April and September, 1979–2015 (monthly average) A linear fit predicts sea ice will disappear in the late summer by the early 2030s (Schweiger et al., 2011 [17]). Data courtesy of PIOMAS (http://psc.apl.uw.edu/research/projects/arctic-sea-ice-volume-anomaly/).

The effects of global warming are felt keenly in the polar regions. The minimum summer extent of Arctic sea ice has more than halved since records began in the 1970s (Wadhams, 2017 [25]) and between 1976 and 1999, its average thickness decreased by 43% (Rothrock, 1999 [16]). Furthermore, it is getting younger: in the 1980s, 'multi-year ice' – ice that has survived at least one melting season – comprised 50–60% of Arctic sea ice; in 2010, just 15% was more than two years old (Comiso, 2012 [5]). Multi-year ice is thicker and more structurally sound than its sister, 'first-year ice', which reaches a maximum thickness of 1.5 m and has unidirectional crystal orientation, making it susceptible to fracture and summer melting. If current rates of decline are sustained, an ice-less summer will be seen within the next decade (see Figure 1 above).

Arctic sea ice begins to grow towards the end of September and thickens over the winter, during which time it receives negligible incoming solar radiation (insolation) due to the polar night. The sun returns in the early spring and ice begins to melt near the beginning

of June. If sea ice is 3 metres thick at the end of the Arctic winter, summer melt is matched by winter growth, so the ice survives the melting season and goes on to become multi-year ice (Wadhams, 2000 [24]). This is desirable: both that it becomes thicker, stronger multi-year ice, and that it is present in the summer, providing its benefits year-round.

These benefits are numerous. Some are localised: sea ice is the predominant habitat of polar bears, a vulnerable species that may see their population reduced by two-thirds if sea ice continues to decline at its current rate (Amstrup et al., 2008 [1]). Preserving Arctic ecosystems is also valuable for its biodiversity in general. Other benefits are global: sea ice increases terrestrial albedo, strengthens the Atlantic meridional overturning circulation (AMOC), and reduces permafrost melt. These effects are explored in great detail in *A Farewell to Ice* (Wadhams, 2017 [25]) and are summarised in the following sections.

1.1.1 Effect on albedo

Albedo is a ratio of reflected to incident solar radiation, measured from 0 (total absorption) to 1 (total reflection). A lower terrestrial albedo implies more radiation is absorbed by the surface of the planet, and hence the rate of global warming increases. With a fresh coat of snow, sea ice has an albedo of around 0.9 – in other words, it reflects 90% of incoming solar radiation. As the snow begins to melt, its albedo reduces to around 0.4. Seawater has an albedo of 0.06. This creates a positive feedback loop, in which sea ice melts, reducing the local albedo, which means that solar radiation is preferentially absorbed in this area, which increases the rate of melting. The reverse is also true, so even a small increase in the area covered by sea ice can be significant.

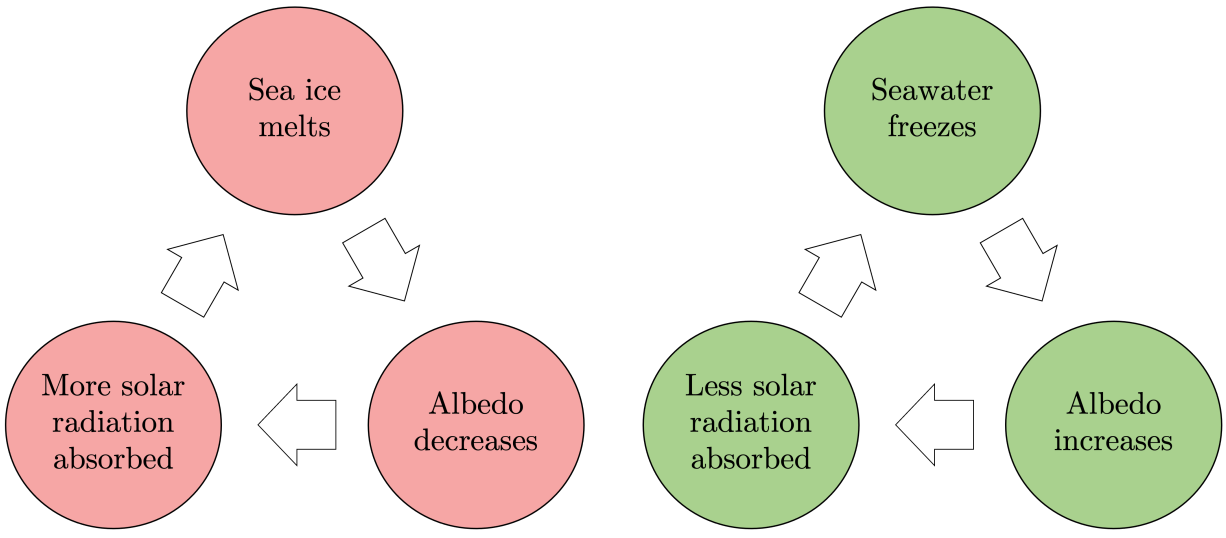

Figure 2: Positive feedback loops associated with sea ice.

1.1.2 Effect on AMOC

The AMOC is a set of currents in the Atlantic Ocean driven by density variations in the different layers of water (which are themselves due to variations in temperature and salinity). The AMOC is responsible for delivering oxygen to deep layers of the ocean and for the relative warmth of the Northern Hemisphere, as well as sequestering $\sim 7 \times 10^8$ tonnes of carbon annually (Gruber et al., 2002 [10]). Sea ice has a lower salt content than the oceans,

so when it melts, the salinity of the oceans reduces, weakening the AMOC (Sévellec et al., 2017 [21]). Effects of AMOC slowdown could include:

- an increase in extreme weather events in the Northern Hemisphere;
- a reduction in the carbon sequestered; and
- complete loss of oxygen to the deep ocean resulting in death of marine life, which would be digested anaerobically by bacteria releasing methane and hydrogen sulphide (Kump et al., 2005 [12]).

1.1.3 Effect on permafrost melt

Beneath the Arctic seabed there is a layer of frozen sediments left over from the ice age. These frozen sediments contain vast quantities of methane, a greenhouse gas 23 times more potent than CO_2. Under just the East Siberian Arctic shelf, there is an estimated 400 Gt of methane trapped in permafrost (Wadhams, 2017 [25]).

It is explained in *A Farewell to Ice* that sea ice acts like an air conditioning system for the ocean. Whilst there is a layer of ice, the temperature of nearby seawater cannot be higher than 0°C – any higher, and energy would be absorbed by the ice as latent heat, cooling the seawater in the process. Consequently, if there is sea ice in the Arctic year-round, the upper layer of the ocean, known as 'polar surface water', never exceeds 0°C. However, more recently, summer sea ice has retreated and polar surface water has reached temperatures as high as 17°C. The permafrost is thawed by warm water and releases the trapped methane. An estimated 50 Gt could be released within a few years of this warming process gathering pace, which would cause a global temperature rise of 0.6°C (Shakhova et al., 2010 [18]).

1.2 The 'ice volcano' as a means to regenerate sea ice

Geoengineering is an umbrella term for an array of techniques that seek to counteract climate change by altering natural systems on a global scale. Using geoengineering to restore Arctic sea ice has been proposed before. Examples include covering ice with reflective glass beads that increase its albedo, to reduce melting (Field et al., 2018 [9]), and flooding existing ice floes with seawater, which then freezes and thickens the ice (Desch et al., 2017 [7]).

Solutions to regenerate the ice fall into two broad categories. Either we can reduce the insolation to which it is exposed in the summer, or we can increase its production in the winter. This report investigates a solution belonging to the latter category, known as the 'ice volcano', which is similar in principle to flooding. The main difference is that in flooding, seawater is pumped onto existing, flat ice floes; in an ice volcano seawater is pumped over a floating conical buoy. The water then flows down and freezes in the cold Arctic atmosphere. By use of a slotted pipe, water can be pumped higher and higher onto the cone of newly-formed ice until it reaches a height of 3 m, at which point it is likely to survive a summer melting season and may provide the benefits outlined in Section 1.1 year-round (Wadhams, 2000 [24]). There is no significant advantage to the ice being thicker than this, as it has the most influence by simply being present. So, once 3 m has been achieved, it is preferable to move onto a new area and begin a new patch of ice. The ice volcano could be powered by nearby wind turbines. Figure 3 illustrates a simple design.

Such a method is attractive because it merely enhances the natural process of ice formation – unlike other geoengineering proposals, it does not require chemicals (e.g. injection of sulphate aerosols into the atmosphere) or weather modification (e.g. marine cloud brightening)

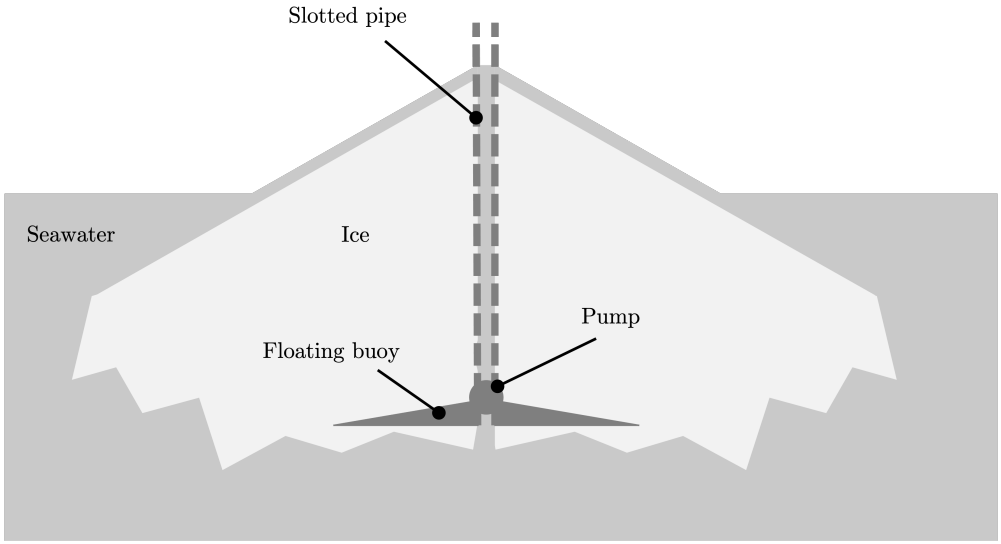

Figure 3: Diagram of an ice volcano. Seawater is pumped from below onto a floating buoy, where it then freezes into a conical 'volcano'. A slotted pipe allows water to be pumped higher as the ice builds up. The vertical scale is exaggerated.

that could have broader, undesirable consequences (Corner and Pidgeon, 2010 [6]; Sovacool, 2021 [20]). Compared to flooding existing sea ice, an ice volcano has two principal advantages. Firstly, it would allow for the creation of new ice floes, rather than just thickening existing ones. Secondly, flooding could result in puddles of biological communities growing on the ice surface (Miller et al., 2020 [15]). These communities would release reactive material that increases atmospheric aerosol loading and warms the Arctic in winter (Willis et al., 2018 [27]). For a conical ice volcano, all excess water should run off without forming puddles, resolving this issue.

Some research into ice volcanoes is already underway. Sev Clarke has investigated practicalities for the design and placement of 'ice shield arrays' (Clarke, 2016 [4]) which are fundamentally the same as ice volcanoes. Daniel Siromani, a summer research student in the Centre for Climate Repair at Cambridge, evaluated the expected ice build-up from an ice volcano over a winter, under the title *Flow of Freezing Salt Water Down a Shallow Conical Slope*. This project extends the work of Clarke and Siromani analytically, by considering the effect of seawater being above its freezing temperature, and also by testing the concept experimentally. The report begins with a mathematical assessment of the problem from first principles. A two-dimensional model is used to predict the ice profiles generated when water is supplied at and above its freezing temperature. The paper *Phase changes following the initiation of a hot turbulent flow over a cold solid surface* (Huppert, 1989 [11]) is used as a basis for this analysis. The two-dimensional model is then tested experimentally. The report concludes with a summary of the results, implications for the deployment of ice volcanoes, and suggestions for further work on the topic.

2 Theory

Nomenclature

α_i	thermal diffusivity of ice
α_w	thermal diffusivity of water
λ_i	thermal conductivity of ice
λ_w	thermal conductivity of water
ρ_i	density of ice
ρ_w	density of water
c_{pi}	specific heat capacity of ice
c_{pw}	specific heat capacity of water
h	coefficient of heat transfer between water and ice
L	specific latent heat of fusion of water
T_f	freezing temperature of fresh water

Where a numerical parameter is required (e.g. in graphs), these are the values used:

$\alpha_i = 1.18 \times 10^{-6}$ m^2/s	$c_{pw} = 4.2$ kJ/kgK
$\alpha_w = 0.132 \times 10^{-6}$ m^2/s	$d = 0.36$ mm
$\lambda_i = 2.22$ W/mK	$h = 2757$ W/m^{2}K
$\lambda_w = 0.56$ W/mK	$L = 334$ kJ/kg
$\rho_i = 916.2$ kg/m^3	$T_f = 273$ K
$\rho_w = 1000$ kg/m^3	$T_{i0} = 255$ K
$c_{pi} = 2.1$ kJ/kgK	$v = 0.6$ m/s

The ice volcano cannot be understood mathematically without first understanding the underlying principles of freezing. In this chapter, a theoretical model is developed that predicts the behaviour of an ice volcano for two fundamental cases: water at its freezing temperature, and water above its freezing temperature. The model has two major simplifications:

- Rather than the full three-dimensional cone, we consider a two-dimensional 'slice' i.e. a sloped channel of zero width.
- All water and ice is treated as fresh, therefore having constant (and equal) melting and freezing temperatures.
- Evaporation, convection and radiation from the water to the atmosphere are ignored.

The model is illustrated in Figure 4. Water enters at a constant temperature T_{w0} at the top of the channel and flows over a semi-infinite slab of cold ice. The upper surface of the ice has a slope of small angle ϕ, that allows the water to flow steadily and parallel to the slope. The boundary between the two evolves as water freezes or ice melts, varying with time and distance along the slope. Mathematically, this is a variation on the classical Stefan problem – a set of partial differential equations that describe the development of a boundary between two states of matter, which are undergoing phase changes.

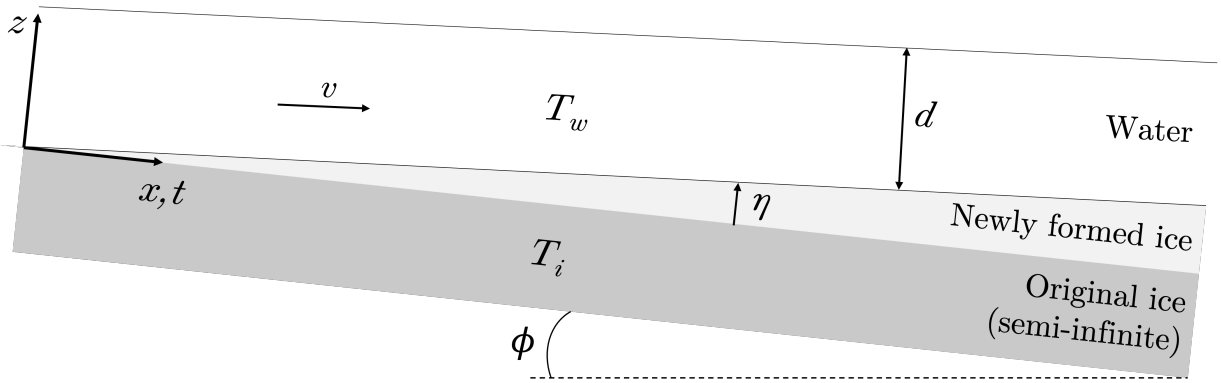

Figure 4: Theoretical model: a steady flow of water down a slope of small angle ϕ, over cold semi-infinite ice.

The primary weakness of this model is its simplification from cone to slice. If it is assumed that the mass flow of water is steady (and large enough that its variations due to melting/freezing are negligible), then the mass flow per unit length would be constant in this two-dimensional model. However, for a three-dimensional cone, the mass flow per unit area would decrease with radius. Siromani indicated that this would cause a transition from sheet flow to rivulet formation at some distance along the slope. Analysis of rivulet formation and its effect on an ice volcano are beyond the scope of this project, but would make a good basis for further investigation.

Ignoring heat transfer to the atmosphere is sensible over short timescales and for warm water, because in these scenarios this accounts for a negligible quantity of heat transfer away from the water. This is verified at the end of this chapter. We may expect this approximation to fail over longer time periods, as the conductive flux to the ice becomes weaker. Other discrepancies in the model will occur due to effects of salinity and finite ice thickness, but these are likely to be less noticeable, at least over short timescales.

2.1 Establishing the general case

First, establish a set of variables. Using the notation of Figure 4:

- x is defined along the original ice slope, and $x = 0$ describes the point where water enters the channel;
- z is defined perpendicular to the original slope, and $z = 0$ describes the initial position of the upper ice surface;
- water first enters the channel at $t = 0$;
- $\eta(x, t)$ is the position of the ice-water boundary, defined in the z-direction;
- $T_i(x, z, t)$ is the the temperature profile of the ice, defined for $z \leq \eta$;
- $T_w(x, z, t)$ is the temperature profile of the water, defined for $z \geq \eta$;
- v is the flow velocity in the x-direction (assumed uniform and constant);
- d is the film depth of the flow (assumed uniform and constant); and
- ϕ is a small angle whose only purpose is to permit steady, gravity-driven flow down the slope. It will therefore be ignored in the following analysis and diagrams.

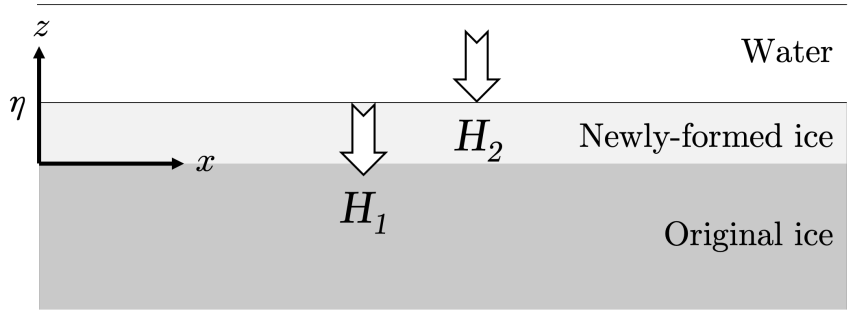

Figure 5: Illustration of heat fluxes at the ice-water interface. H_1 is a conductive heat flux down into the ice, away from the interface; H_2 is a convective heat flux from the water to the ice.

Please note that in the following diagrams, the y-axis always represents z, but the x-axis represents several different variables depending on the context (x, t, T_i and T_w) which are labelled in the individual figures.

All figures in this report are original unless otherwise stated.

Let us consider the situation at hand: (relatively warm) water flows over (relatively cold) ice. At the interface, two heat fluxes are induced, illustrated in Figure 5. Firstly, a conductive heat flux per unit length, say H_1, within the ice, away from the interface, and proportional to the local temperature gradient:

$$H_1(x,t) \propto \left.\frac{\partial T_i}{\partial z}\right|_{z=\eta} = \lambda_i \left.\frac{\partial T_i}{\partial z}\right|_{z=\eta} \tag{1}$$

Secondly, a convective heat flux per unit length, say H_2, from the water to the ice, and proportional to the temperature difference between the bulk fluid and the interface:

$$H_2(x,t) \propto (T_w - T_{interface}) = h(T_w - T_{interface}) \tag{2}$$

Latent heat will also be released as water freezes, or absorbed as ice melts. The behaviour of the system is governed by these three processes.

2.1.1 Behaviour at $t = 0^+$

The ice is initially at a uniform temperature, say T_{i0}, which is less than the freezing temperature of water, T_f. Consider the instant at which water first touches the ice. The temperature profile across the ice-water interface must immediately become continuous. This interfacial temperature cannot exceed T_f, since this would imply that part of the ice had melted instantaneously. Likewise, it cannot be below T_f, since this would imply that some of the water had frozen instantaneously. Therefore, the interface temperature must equal T_f, and will continue to equal T_f (Huppert, 1989 [11]).

$$T_i(x,z,t) = T_w(x,z,t) = T_f \qquad (z = \eta)$$

We defined z such that $z = 0$ corresponds to the upper ice surface at $t = 0$. From the instant at which water first touches the ice, this surface becomes the ice-water interface, and thus must instantaneously change temperature at $t = 0$ from T_{i0} to T_f (see Figure 6):

$$T_i(x,z,t) = T_{i0} \qquad (z = 0, \quad t < 0)$$

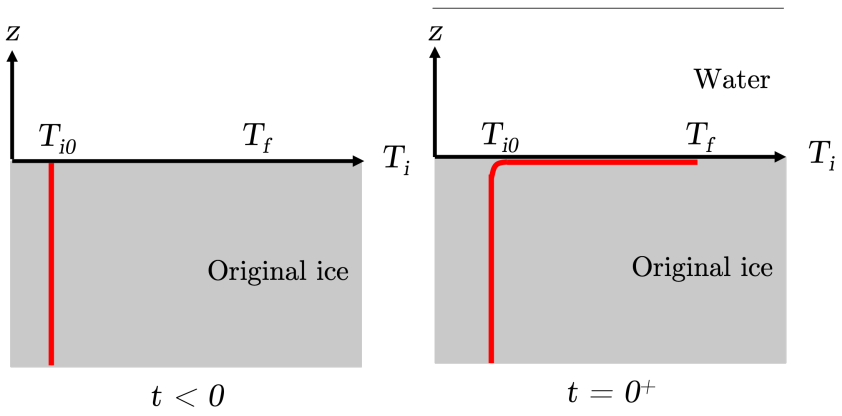

Figure 6: Plots of T_i against z for $t < 0$ and $t = 0^+$. At $t = 0^+$, the interface must assume T_f, creating a temperature profile that tends to a step function and a temperature gradient that at $z = 0$ tends to an infinite value. Note that the x-axis here represents the temperature in the ice.

$$T_i(x, z, t) = T_f \qquad (z = 0, \quad t = 0^+)$$

Just below the surface, however, the temperature at $t = 0^+$ is still T_{i0}, because the temperature signal has not yet had time to propagate downwards. At this instant, the temperature gradient at the interface takes a very large value that tends to infinity.

$$\left.\frac{\partial T_i}{\partial z}\right|_{z=\eta} \to \infty \qquad (t = 0^+)$$

The conductive heat flux in the ice, H_1, is proportional to this temperature gradient, and thus also initially tends to infinity, from Equation (1).

$$H_1 = \lambda_i \left.\frac{\partial T_i}{\partial z}\right|_{z=\eta} \to \infty \qquad (t = 0^+)$$

The convective heat flux into the interface, H_2, is proportional to the temperature difference between the water and the interface, so must be finite and non-negative. Therefore, the conductive heat flux may only be balanced by a release of latent heat – freezing of some water – initially at a very fast rate, tending towards infinity.

No constraints have been placed on the temperature of the water, so this analysis gives the rather intriguing result that, irrespective of the initial water temperature, and for ice initially below the phase change temperature, freezing must be the initial response. This was previously shown in *Phase changes following the initiation of a hot turbulent flow over a cold solid surface* (Huppert, 1989 [11]).

2.1.2 Behaviour as the problem develops

Let us continue to analyse the heat fluxes at the ice-water interface. Consider the control volume of Figure 7, which encompasses a section of the interface over a time δt. Applying the first law of thermodynamics:

$$H_2(x, t)\delta t - H_1(x, t)\delta t + \rho_i L \left[\eta(x, t + \delta t) - \eta(x, t)\right] = 0$$

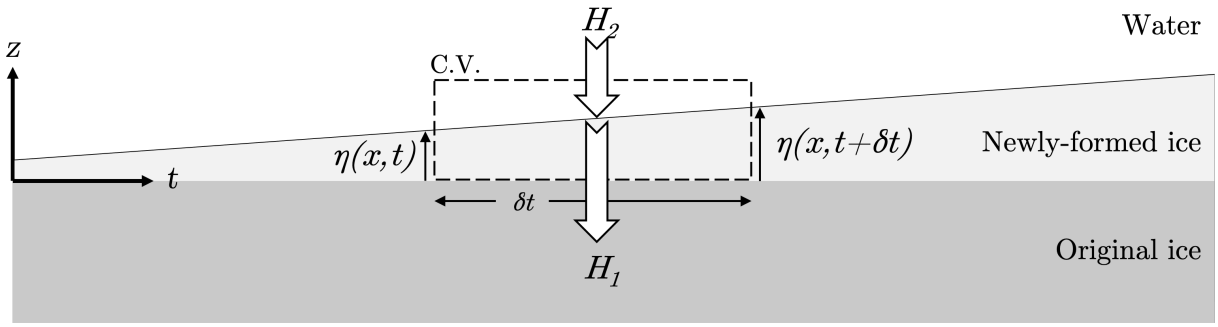

Figure 7: Control volume encompassing a section of the interface from a time t to $t + \delta t$. The heat fluxes H_1 and H_2 are also shown. Note that the x-axis here represents time.

$$\rho_i L \left[\frac{\eta(x, t + \delta t) - \eta(x, t)}{\delta t} \right] = H_1(x, t) - H_2(x, t)$$

Taking the limit as $\delta t \to 0$ and substituting in (1) for H_1 (for now, it is more convenient to leave H_2 as is), the heat flux equation becomes

$$\rho_i L \frac{\partial \eta}{\partial t} = \lambda_i \left. \frac{\partial T_i}{\partial z} \right|_{z=\eta} - H_2(x, t) \tag{3}$$

which is known as the Stefan condition. The development of the ice profile may now be explained qualitatively by the relationship between H_1 and H_2, each of which will always take a non-negative value. If H_1 exceeds H_2, $\frac{\partial \eta}{\partial t}$ is positive and the ice thickens (freezing). Conversely, if H_2 exceeds H_1, $\frac{\partial \eta}{\partial t}$ is negative and the ice thins (melting).

Initially, as determined in Section 2.1.1, H_1 tends to infinity and H_2 is finite, initially resulting in ice growth at a very fast rate that tends to infinity. However, with increasing time, the conductive temperature gradient in the ice weakens, H_1 reduces, and the rate of freezing decreases.

What happens next depends on the temperature of the water. This will be discussed in the following two sections.

2.2 Water initially at its freezing temperature

If the water enters the channel at its freezing temperature, T_f, the problem reduces to what is known as a 'one-phase Stefan problem'. Essentially, the water may react in one of two ways: it may remain liquid, and remain at T_f, or it may freeze (and then cool further). Either way, any water present must be at T_f, and the temperature profile in the water may be represented by a constant:

$$T_w(x, z, t) = T_f$$

The water may not cool whilst also remaining liquid, so any variation leads to a phase change. The water phase can then be neglected mathematically (hence 'one-phase'), significantly simplifying the analysis.

Since the interface temperature and the water temperature are both equal to T_f, there is no convective heat flux from the water to the ice, i.e. $H_2 = 0$. They are also both constant and uniform in (x, z, t), so the ice, which has a uniform temperature in (x, z) for $t < 0$, effectively

'sees' the same boundary condition at the interface all along its length in the x-direction. Hence the ice temperature is independent of x, as is the position of the interface.

$$T_i = T_i(z,t) \qquad \eta = \eta(t)$$

This indicates that the ice build-up should be uniform in the x-direction, for water initially at T_f. At any given position along the slope, the change in ice thickness should be the same.

Let us explore this mathematically. The Stefan condition, Equation (3), becomes:

$$\rho_i L \frac{\mathrm{d}\eta}{\mathrm{d}t} = \lambda_i \left. \frac{\partial T_i}{\partial z} \right|_{z=\eta} \tag{4}$$

since $H_2 = 0$. This indicates that $\frac{\mathrm{d}\eta}{\mathrm{d}t}$ is exclusively non-negative and reduces with time from a value that initially tends to infinity, as the temperature gradient in the ice weakens.

The ice temperature is governed by the transient heat diffusion equation

$$\frac{\partial T_i}{\partial t} = \alpha_i \left(\frac{\partial^2 T_i}{\partial x^2} + \frac{\partial^2 T_i}{\partial z^2} \right)$$

but since $T_i = T_i(z,t)$ only, this becomes

$$\frac{\partial T_i}{\partial t} = \alpha_i \frac{\partial^2 T_i}{\partial z^2} \tag{5}$$

We can write down two boundary conditions immediately. Before water enters the channel, the ice is at a uniform temperature T_{i0}, and the ice-water interface is always at T_f:

$$T_i(z,t) = T_{i0} \qquad (t < 0)$$

$$T_i(z,t) = T_f \qquad (z = \eta)$$

To find the third, consider the far-field in the negative z-direction, where the ice temperature is still equal to T_{i0}:

$$T_i(z,t) = T_{i0} \qquad (z \to -\infty)$$

It is convenient to non-dimensionalise Equations (4) and (5) by introducing a set of dimensionless variables:

$$Z = \frac{z}{l} \qquad X = \frac{x}{l} \qquad \tau = \frac{\alpha_i t}{l^2}$$

$$H(\tau) = \frac{\eta(t)}{l} \qquad \theta_i(Z,\tau) = \frac{T_i(z,t) - T_f}{T_{i0} - T_f} \qquad St_i = \frac{c_{pi}(T_{i0} - T_f)}{L}$$

where T_f, T_{i0}, c_{pi}, α_i, and L are as defined previously, and l is a characteristic length scale of the problem. With the introduction of these variables, Equation (4) becomes:

$$\frac{\mathrm{d}H}{\mathrm{d}\tau} = St_i \left. \frac{\partial \theta_i}{\partial Z} \right|_{Z=H} \tag{6}$$

and Equation (5) becomes:

$$\frac{\partial \theta_i}{\partial \tau} = \frac{\partial^2 \theta_i}{\partial Z^2} \tag{7}$$

with boundary conditions

$$\theta_i(Z,\tau) = 1 \qquad (\tau < 0) \tag{8}$$

$$\theta_i(Z,\tau) = 0 \qquad (Z = H) \tag{9}$$

$$\theta_i(Z,\tau) = 1 \qquad (Z \to -\infty) \tag{10}$$

Assuming a temperature profile on the basis of heat conduction in a semi-infinite body, the general solution to Equation (7) is

$$\theta_i(Z,\tau) = A + B\,\mathrm{erf}\left(\frac{Z}{2\sqrt{\tau}}\right) \tag{11}$$

where A and B are unknown constants to be determined. By substitution of the boundary condition (10), obtain

$$\theta_i(Z \to -\infty, \tau) \quad = \quad A + B\,\mathrm{erf}\,(-\infty) \quad = \quad A - B \quad = \quad 1$$

so, $A = 1 + B$. Substitute this back into (11):

$$\theta_i(Z,\tau) = (1+B) + B\,\mathrm{erf}\left(\frac{Z}{2\sqrt{\tau}}\right)$$

Let us consider the temperature at the interface, by substitution of boundary condition (9):

$$\theta_i(Z = H, \tau) = (1+B) + B\,\mathrm{erf}\left(\frac{H}{2\sqrt{\tau}}\right) = 0$$

Since B is known to be a constant, $\frac{H}{2\sqrt{\tau}}$ must also be a constant for the equation above to hold. Label this constant γ, such that:

$$\gamma = \frac{H}{2\sqrt{\tau}} \tag{12}$$

and thus

$$(1+B) + B\,\mathrm{erf}\,\gamma = 0 \quad \Rightarrow \quad B = -\frac{1}{1+\mathrm{erf}\,\gamma}$$

$$A \quad = \quad 1 + B \quad = \quad \frac{\mathrm{erf}\,\gamma}{1+\mathrm{erf}\,\gamma}$$

$$\theta_i(Z,\tau) = \frac{\mathrm{erf}\,\gamma - \mathrm{erf}\left(\frac{Z}{2\sqrt{\tau}}\right)}{1+\mathrm{erf}\,\gamma} \tag{13}$$

The value of the constant γ determines the temperature profile of the ice and governs the formation of ice in the channel.

2.2.1 Ignoring the contribution of the moving interface

As water flows over the ice, heat is transferred to the ice and conducted downwards. Some water then freezes, and the ice-water interface moves upwards. Due to this movement, the

heat now must be conducted a little further to reach an equivalent depth. But suppose that we ignore the extra distance the heat must be conducted, and assume that heat transfer between ice and water always takes place at the original interface position (at $z = 0$). This approximation will be referred to as 'ignoring the moving interface'.

When the net change in ice thickness is positive (i.e. the interface has moved upwards), this approximation will overestimate the amount of freezing. This is because the distance from the interface (at T_f) to far-field ice (at T_{i0}) is further in reality than it is in the model, so the model predicts a steeper temperature gradient in the ice (which corresponds to a faster rate of freezing). When the net change in ice thickness is negative (i.e. the interface has moved downwards), this approximation will underestimate the amount of freezing (or overestimate the amount of melting), since the model predicts a shallower temperature gradient than in reality. This approximation is therefore conservative for net melting and exaggerated for net freezing.

Mathematically, ignoring the moving interface is equivalent to altering Equation (6), the dimensionless Stefan condition, to

$$\frac{\mathrm{d}H}{\mathrm{d}\tau} = St_i \frac{\partial \theta_i}{\partial Z}\bigg|_{Z=0} \tag{14}$$

and boundary condition (9) to

$$\theta_i(Z, \tau) = 0 \qquad (Z = 0)$$

This implies $\gamma = 0$, and thus Equation (13) becomes

$$\theta_i(Z, \tau) = -\operatorname{erf}\left(\frac{Z}{2\sqrt{\tau}}\right) \tag{15}$$

Substitution of (15) into (14) yields

$$\frac{\mathrm{d}H}{\mathrm{d}\tau} = -\frac{St_i}{\sqrt{\pi\tau}}$$

As forecast in Section 2.1.1, the initial rate of ice formation tends towards infinity. The above equation can be integrated to find the overall change in ice thickness with time:

$$H(\tau) = -\frac{2St_i}{\sqrt{\pi}}\sqrt{\tau}$$

or, in dimensional terms

$$\boxed{\eta(t) = \frac{2c_{pi}(T_f - T_{i0})}{L\sqrt{\pi}}\sqrt{\alpha_i t}} \tag{16}$$

This model is valid for changes in ice thickness that are small in comparison with the characteristic propagation distance of the temperature signal, e.g. for large latent heat of fusion L or large thermal diffusivity α_i.

2.2.2 Including the contribution of the moving interface

A more accurate result can be obtained by accounting for the moving interface when calculating the conductive temperature profile in the ice (i.e. by assuming that heat transfer between water and ice always takes place at the true interface position).

Recall Equations (6), (12), and (13) respectively:

$$\frac{\partial H}{\partial \tau} = St_i \frac{\partial \theta_i}{\partial Z}\bigg|_{Z=H} \qquad \gamma = \frac{H}{2\sqrt{\tau}} \qquad \theta_i(Z,\tau) = \frac{\operatorname{erf}\gamma - \operatorname{erf}\left(\frac{Z}{2\sqrt{\tau}}\right)}{1+\operatorname{erf}\gamma}$$

Substituting (12) and (13) into (6) gives the transcendental equation

$$\gamma = -\frac{St_i}{\sqrt{\pi}} \frac{e^{-\gamma^2}}{1+\operatorname{erf}\gamma} \tag{17}$$

where the dimensionless constant γ now depends only on St_i. The position of the ice-water interface (which is equivalent to the change in ice thickness) is then given from (12) by

$$H(\tau) = 2\gamma\sqrt{\tau} \quad \text{or, in dimensional terms,} \quad \boxed{\eta(t) = 2\gamma\sqrt{\alpha_i t}} \tag{18}$$

giving a rate of ice formation that initially tends to infinity, as expected.

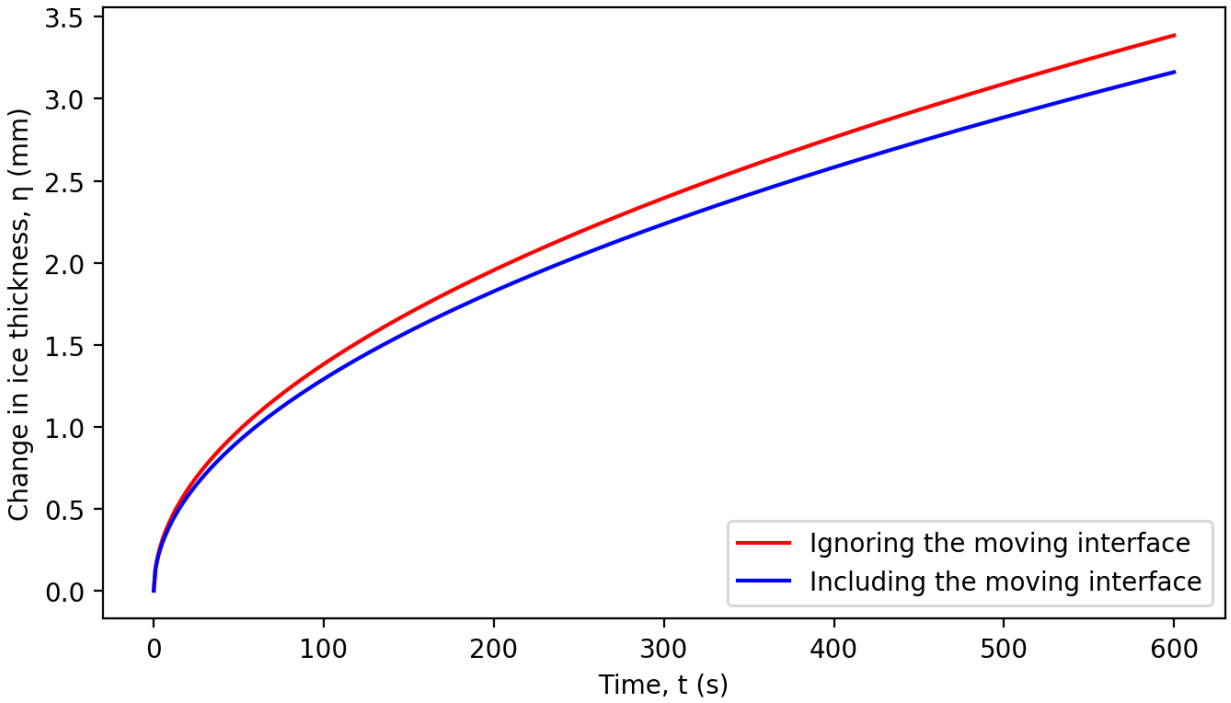

Figure 8: Theoretical variation of ice thickness with time, ignoring the moving interface (red) and including the moving interface (blue). Ignoring the moving interface slightly overestimates the ice formation, as predicted. This is because using this approximation gives an overestimation for the temperature gradient in the ice (for net freezing).

A Newton-Raphson method coded in Python was used to solve for γ from Equation (17) and the resulting ice profile plotted, along with the result from Section 2.2.1 (the 'no moving

interface' model). Marginally less freezing is predicted when the moving interface is being included, but the difference is small. After 10 minutes, 3.16 mm of ice is predicted by the moving interface model and 3.39 mm is predicted by the simple model – a percentage difference of 7%. In comparison, the characteristic distance propagated by the temperature signal, $z \sim \sqrt{\alpha_i t}$, is 27 mm after 10 minutes, which is almost an order of magnitude larger. It is therefore considered reasonable to continue neglecting the moving interface for water initially warmer than the freezing temperature, provided T_w is close to T_f such that any change in ice thickness due to melting is small (since we have already shown that the change in ice thickness due to freezing is sufficiently small).

For water initially at its freezing temperature, the key results (true for both models) are that only freezing will occur; the ice thickness, η, should increase proportionally to the square root of t:

$$\boxed{\eta(t) \propto \sqrt{t}}$$

and that ice build-up is uniform, i.e. independent of distance along the slope. For any x, we expect the change in ice thickness to be equivalent.

2.3 Water initially warmer than the freezing temperature

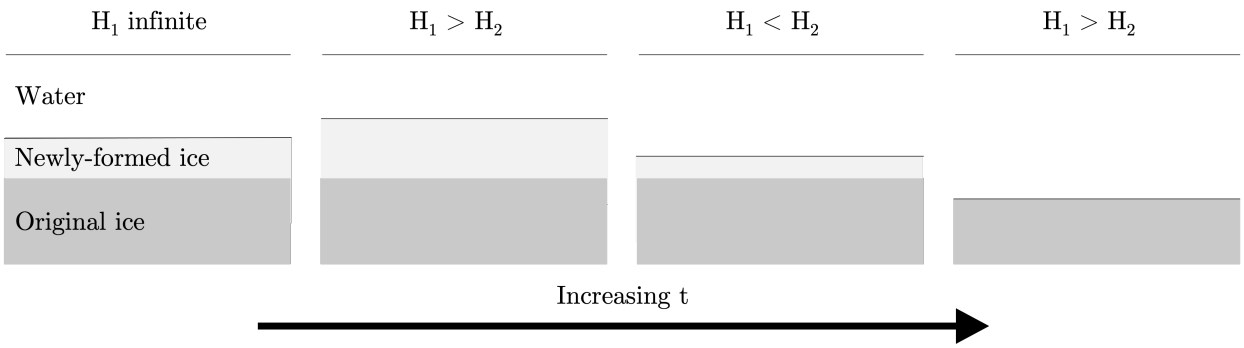

Figure 9: From left to right (with increasing time): initially very large H_1 and very rapid freezing; H_1 reduces (but still exceeds H_2) and rate of freezing slows; H_2 exceeds H_1 and newly-formed ice begins to melt; $H_2 > H_1$, newly-formed ice has all melted and original ice begins to melt.

The previous section dealt with water entering the channel at its freezing temperature, T_f. Let us now consider water entering at a warmer temperature, T_{w0}.

$$T_w(x, z, t) = T_{w0} > T_f \qquad (x = 0)$$

With a warmer inlet temperature, freezing and melting can both occur. We begin with a qualitative analysis. As before, the conductive heat flux within the ice, H_1, initially tends to infinity. This initially leads to freezing at a very fast rate that tends to infinity. As the temperature gradient in the ice weakens with time, H_1 decreases, and the rate of freezing slows. This continues until H_1 is exceeded by the convective heat flux from the water to the ice, H_2, at which point the ice starts to melt, beginning with the newly-formed ice, followed by the original ice (once the newly-formed ice has melted). Figure 9 illustrates this timeline.

The problem will now be examined mathematically. At the end of Section 2.1.2, the gov-

erning equation at the interface (the Stefan condition) was found to be:

$$\rho_i L \frac{\partial \eta}{\partial t} = \lambda_i \frac{\partial T_i}{\partial z}\bigg|_{z=\eta} - H_2(x,t)$$

from Equation (3). In the previous section, the 'no moving interface' assumption was deemed valid for small changes in ice thickness. For T_{w0} close to the freezing temperature, the change in ice thickness will due to melting is indeed small, so the assumption is permitted. The Stefan condition then becomes

$$\rho_i L \frac{\partial \eta}{\partial t} = \lambda_i \frac{\partial T_i}{\partial z}\bigg|_{z=0} - H_2(x,t) \tag{19}$$

Conductive heat transfer in the ice is again governed by the transient diffusion equation

$$\frac{\partial T_i}{\partial t} = \alpha_i \left(\frac{\partial^2 T_i}{\partial x^2} + \frac{\partial^2 T_i}{\partial z^2} \right)$$

except T_i is no longer known to be independent of x. Assume that the velocity of the flow is much larger than the characteristic velocity of the temperature signal in the ice, i.e.

$$v >> \sqrt{\frac{\alpha_i}{t}}$$

such that propagation of heat in the x-direction can be neglected, giving the relationship

$$\frac{\partial T_i}{\partial t} = \alpha_i \frac{\partial^2 T_i}{\partial z^2} \tag{20}$$

as for the freezing temperature case, with boundary conditions

$$T_i(x,z,t) = T_{i0} \qquad (t < 0) \tag{21}$$

$$T_i(x,z,t) = T_f \qquad (z = 0) \tag{22}$$

$$T_i(x,z,t) = T_{i0} \qquad (z \to -\infty) \tag{23}$$

Note that (22) is defined at $z = 0$, rather than $z = \eta$, since the moving interface is being neglected. It is again convenient to non-dimensionalise Equation (20) using the same dimensionless variables as in Section 2.2, giving

$$\frac{\partial \theta_i}{\partial \tau} = \frac{\partial^2 \theta_i}{\partial Z^2} \tag{24}$$

with boundary conditions

$$\theta_i(X,Z,\tau) = 1 \qquad (\tau < 0) \tag{25}$$

$$\theta_i(X,Z,\tau) = 0 \qquad (Z = 0) \tag{26}$$

$$\theta_i(X,Z,\tau) = 1 \qquad (Z \to -\infty) \tag{27}$$

as before. From the above assumption that propagation of heat within the ice in the x-direction is negligible, assume a separable solution in X and in (Z,τ) for the ice temperature

profile:

$$\theta_i(X, Z, \tau) = F(X)G(Z, \tau)$$

Assuming that G has a temperature profile on the basis of heat conduction in a semi-infinite body, the general solution to Equation (24) is

$$\theta_i(X, Z, \tau) = F(X)\left[A + B\,\mathrm{erf}\left(\frac{Z}{2\sqrt{\tau}}\right)\right] \tag{28}$$

Substitution of boundary condition (26) into the general solution (28) gives

$$\theta_i(X, Z = 0, \tau) = F(X)A = 0$$

implying $A = 0$, since $F(X) = 0$ would mean $\theta_i = 0$ at all times, which cannot be the case as we have defined $T_{i0} < T_f$. So,

$$\theta_i(X, Z, \tau) = F(X)\left[B\,\mathrm{erf}\left(\frac{Z}{2\sqrt{\tau}}\right)\right]$$

Substitution of the boundary condition (23) then gives

$$\theta_i(X, Z \to -\infty, \tau) = F(X)[-B] = 1$$

$$\Rightarrow \quad B = -\frac{1}{F(X)}$$

Simplification leads to an equation for the temperature profile in the ice:

$$\theta_i(X, Z, \tau) = F(X)\left[-\frac{1}{F(X)}\,\mathrm{erf}\left(\frac{Z}{2\sqrt{\tau}}\right)\right] = -\,\mathrm{erf}\left(\frac{Z}{2\sqrt{\tau}}\right)$$

$$\Rightarrow \quad T_i(x, z, t) = T_f + (T_f - T_{i0})\,\mathrm{erf}\left(\frac{z}{2\sqrt{\alpha_i t}}\right) \tag{29}$$

Note that T_i is again a function of (z, t) only. This is the same result as in Section 2.2.1. Substitute (29) back into the Stefan condition, Equation (19), to find the a differential equation governing the ice thickness:

$$\rho_i L\frac{\partial \eta}{\partial t} = \frac{\lambda_i(T_f - T_{i0})}{\sqrt{\pi\alpha_i t}} - H_2(x, t) \tag{30}$$

By finding an expression for $H_2(x, t)$, this equation can be solved for η.

2.3.1 Ignoring the thermal boundary layer in the fluid

As the (relatively warm) water flows over the ice, a thermal boundary layer is established, outside of which the water temperature is equal to its inlet temperature, T_{w0}. For this first model, we will ignore the thermal boundary layer, assuming that the water is well-mixed in the z-direction (but not the x-direction); in other words, T_w is independent of z. Figure 10 illustrates the approximate water temperature profile for this model alongside the one with the boundary layer included (which will be analysed in the following section).

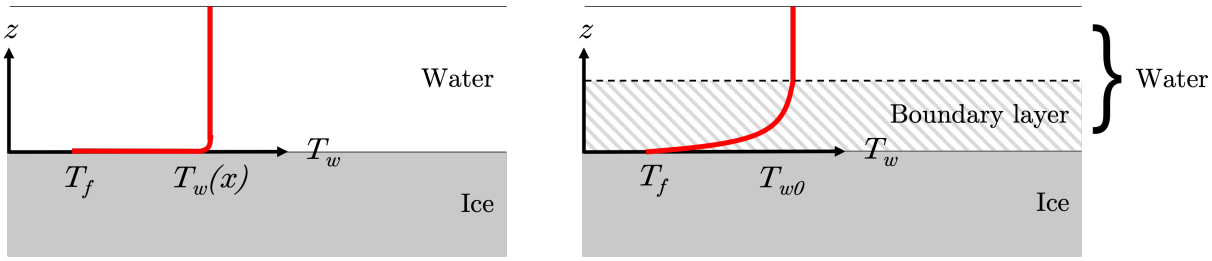

Figure 10: Illustration of the temperature profile in the water, ignoring the thermal boundary layer (left) and including the thermal boundary layer (right). Note that the x-axis here represents the water temperature.

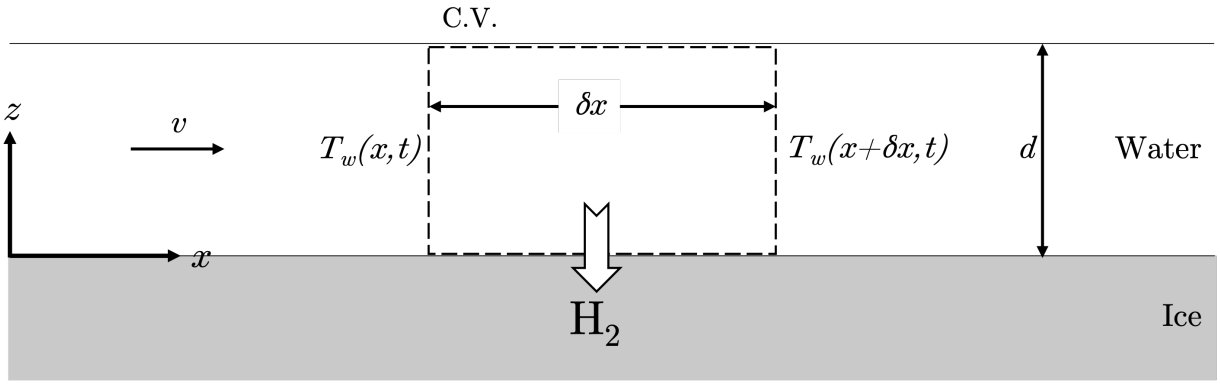

Figure 11: Control volume encompassing a chunk of water of height d from x to $x + \delta x$. The convective heat flux to the ice, H_2, is included. Note that the x-axis here represents x.

Consider the control volume of Figure 11, which encompasses a chunk of water of length δx and height d (the full depth of the flow). The chunk is subject to H_2, the convective heat flux from the water to the ice, which causes a change in temperature. We recall that H_2 was defined in Equation (2) as $h(T_w - T_{interface})$. Assume that the mass flow rate is sufficiently large that variations due to melting and freezing are negligible, such that the water velocity, v, and depth, d, may be considered uniform and constant (Towell and Rothfeld, 1966 [22]).

It is useful to first consider the problem qualitatively. The water temperature, T_w, is a function only of the rate of heat transfer away from the water. The rate of heat transfer away from the water is H_2 per unit length, and H_2 depends only on T_w. The water enters the channel at T_{w0} for all t, so at $x = 0$, H_2 does not depend on t. Just past $x = 0$, the water temperature cannot depend on t, because the heat transfer it has experienced, that has caused the change in temperature, does not depend on t. Therefore, H_2 cannot depend on t just past $x = 0$, because the water temperature just past $x = 0$ does not depend on t, and so on, until it becomes clear that T_w and H_2 do not have any time dependence at all, only x-dependence. This is an important result.

We may write

$$H_2 = H_2(x)$$
$$T_w = T_w(x) \qquad (z > 0)$$

since we have shown that T_w is independent of t, and neglecting the thermal boundary layer in the water means that T_w is also independent of z – though at $z = 0$, the assumed interface

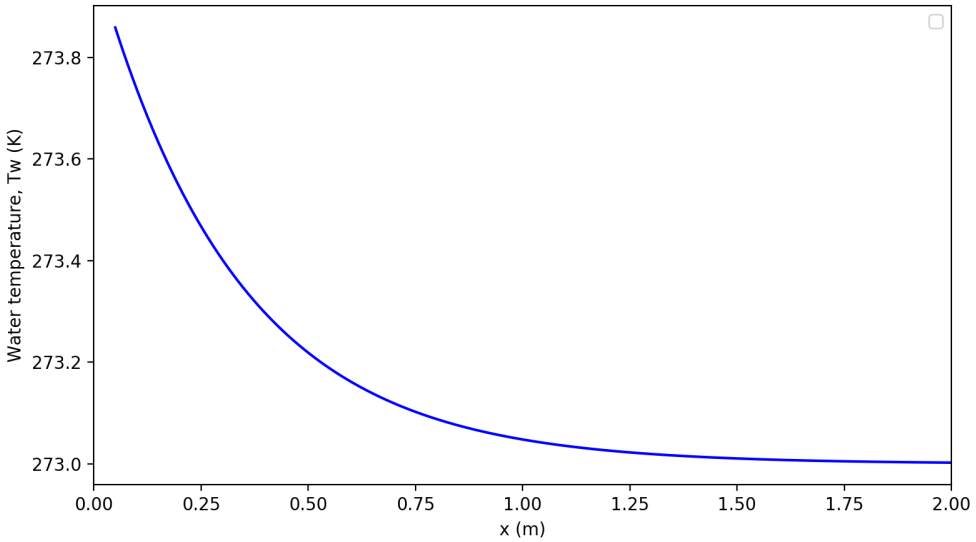

Figure 12: Variation of T_w with x, ignoring the thermal boundary layer, for $T_{w0} = 274$ K. The water temperature decreases exponentially towards an asymptote of T_f.

position, the temperature will still be T_f (as in Figure 10). The control volume of Figure 11 may now be evaluated mathematically. Applying the first law of thermodynamics, the change in enthalpy must be equal to heat transfer to the control volume:

$$\rho_w v dc_{pw}[T_w(x+\delta x) - T_w(x)] = -H_2(x)\delta x$$

Let us now substitute in for $H_2(x)$ from Equation (2) and divide by δx:

$$\rho_w v dc_{pw}\frac{T_w(x+\delta x) - T_w(x)}{\delta x} = -h[T_w(x) - T_f]$$

Taking the limit as $\delta x \to 0$, and solving:

$$\rho_w v dc_{pw}\frac{\mathrm{d}T_w(x)}{\mathrm{d}x} = -h[T_w(x) - T_f]$$

$$\int_{T_{w0}}^{T_w(x)} \frac{1}{T_w(x) - T_f}\, dT_w = \int_0^x -\frac{h}{\rho_w v dc_{pw}}\, dx$$

$$\ln\frac{T_w(x) - T_f}{T_{w0} - T_f} = -\frac{h}{\rho_w v dc_{pw}}x$$

$$\Rightarrow \quad \frac{T_w(x) - T_f}{T_{w0} - T_f} = \exp\left\{-\frac{h}{\rho_w v dc_{pw}}x\right\} \tag{31}$$

This result describes the water temperature decreasing exponentially with x, tending towards a horizontal asymptote of T_f. Figure 12 shows this result for a water inlet temperature of 274 K. In this model, T_w never actually reaches T_f, because the lower the temperature, the smaller the heat flux out of the water, so the smaller the temperature change.

Equation (31) above can be rewritten as

$$H_2(x) = h(T_w(x) - T_f) = h(T_{w0} - T_f)\exp\left\{-\frac{h}{\rho_w v d c_{pw}}x\right\}$$

to give a result for H_2, as required by Equation (30). H_2 here also decreases exponentially with x. Substitution back into Equation (30) yields an equation describing the change in ice thickness:

$$\rho_i L\frac{\partial \eta}{\partial t} = \frac{\lambda_i(T_f - T_{i0})}{\sqrt{\pi\alpha_i t}} - h(T_{w0} - T_f)\exp\left\{-\frac{h}{\rho_w v d c_{pw}}x\right\} \tag{32}$$

$$\boxed{\eta(x,t) = \frac{1}{\rho_i L}\left[\frac{2\lambda_i(T_f - T_{i0})}{\sqrt{\alpha_i \pi}}\sqrt{t} - h(T_{w0} - T_f)\exp\left\{-\frac{h}{\rho_w v d c_{pw}}x\right\}t\right]} \tag{33}$$

This model is valid for flows well-mixed in the z-direction, e.g. thin film depth d, high thermal diffusivity α_w, high Reynolds number vd/ν.

2.3.2 Including the thermal boundary layer in the fluid

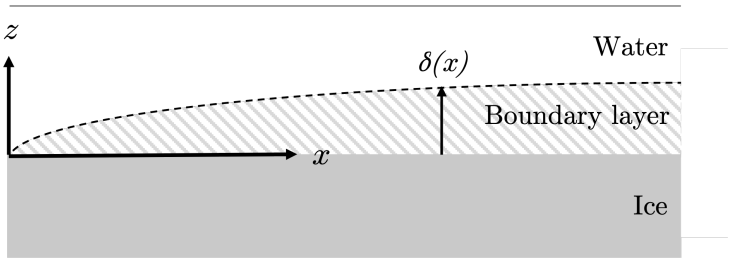

Figure 13: Illustration of the boundary layer in the water, whose thickness scales with $\sqrt{x}$. Note that the x-axis here represents x.

In this section we will account for the thermal boundary layer in the water. The temperature profile in the water is approximately as in Figure 10. At the interface, the water is at T_f. Its temperature then increases through the boundary layer and is the water inlet temperature, T_{w0}, outside the boundary layer. The boundary layer thickness, $\delta(x)$, increases with x (see Figure 13), scaling as

$$\delta(x) \sim \sqrt{\frac{\alpha_w x}{v}}$$

where α_w is the thermal diffusivity of water, and v is the flow velocity in the x-direction. It is now appropriate use a corresponding heat transfer coefficient between water and ice that varies with x:

$$h = h(x) = \lambda_w\sqrt{\frac{v}{\alpha_w x}} \qquad (x > 0) \tag{34}$$

Equation (34) describes the heat transfer coefficient from outside the boundary layer in the water to the ice (i.e. *through* the boundary layer). The boundary layer thickens with $\sqrt{x}$, which means that h decreases with $\sqrt{x}$ (since the heat must be transported through an ever-thickening boundary layer). The temperatures between which the convection takes

place are the water temperature *outside* of the boundary layer (which is constant and equal to the water inlet temperature, T_{w0}) and the interface temperature (at T_f). As before, this means that H_2 is a function of x only.

$$H_2(x) = h(x)(T_{w0} - T_f) = \lambda_w \sqrt{\frac{v}{\alpha_w x}}(T_{w0} - T_f)$$

Substitution into (30) and integration gives the result for η.

$$\rho_i L \frac{\partial \eta}{\partial t} = \frac{\lambda_i (T_f - T_{i0})}{\sqrt{\pi \alpha_i t}} - \lambda_w \sqrt{\frac{v}{\alpha_w x}}(T_{w0} - T_f) \tag{35}$$

$$\boxed{\eta(x,t) = \frac{1}{\rho_i L}\left[\frac{2\lambda_i (T_f - T_{i0})}{\sqrt{\alpha_i \pi}}\sqrt{t} - \lambda_w \sqrt{\frac{v}{\alpha_w x}}(T_{w0} - T_f)t\right]} \tag{36}$$

This model is valid before the boundary layer reaches the full depth of the fluid, which occurs at a position $x \sim vd^2/\alpha_w$ for all t. The model would also break down if the 'no heat transfer to atmosphere' assumption were removed, since the water would be being cooled from above as well as from below. This would result in two growing boundary layers in the water, one at the surface in contact with the air and one at the surface in contact with the ice. The water outside of the ice boundary layer would then no longer be at T_{w0}.

2.3.3 Summary for water initially above its freezing temperature

The graphs in this section have change in ice thickness, η, on the x-axis measured in mm. The y-axis represents either time, t, in seconds; or distance along the channel, x, in m. There is considerable vertical exaggeration.

From Section 2.3.1, the equation governing the rate of change of ice thickness (ignoring the boundary layer) is

$$\rho_i L \frac{\partial \eta}{\partial t} = \frac{\lambda_i (T_f - T_{i0})}{\sqrt{\pi \alpha_i t}} - h(T_{w0} - T_f) \exp\left\{-\frac{h}{\rho_w v d c_{pw}} x\right\} \tag{37}$$

The equivalent equation from Section 2.3.2 (including the boundary layer) is

$$\rho_i L \frac{\partial \eta}{\partial t} = \frac{\lambda_i (T_f - T_{i0})}{\sqrt{\pi \alpha_i t}} - \lambda_w \sqrt{\frac{v}{\alpha_w x}}(T_{w0} - T_f) \tag{38}$$

The two terms on the right-hand sides of Equations (37) and (38) are H_1 and H_2 respectively. The difference between the two determines the rate of change of the ice thickness. In both cases, H_1 decays with $\sqrt{t}$ but has no x-dependence, and H_2 decays with x but has no time-dependence (ignoring the boundary layer, the decay is exponential, and including it, the decay is with $\sqrt{x}$).

At any given position (x constant), H_2 takes a constant, finite value and H_1 decreases with $\sqrt{t}$, from an initial value that is very large and tends to infinity. At $t = 0$, since H_2 is finite, $\frac{\partial \eta}{\partial t}$ must balance H_1, implying very rapid freezing at a rate that tends to infinity.

As H_1 decreases, the rate of freezing slows, until H_2 exceeds H_1 and freezing is replaced by melting (initially of the newly-formed ice, then of the original ice). The time until freezing is replaced by melting depends only on x. Near the channel inlet, H_2 is large, so the time until melting will be relatively low (and vice versa far from the inlet). Therefore, it is expected that a large amount of melting occurs near the inlet, because melting begins sooner, and almost none ever occurs far from the inlet.

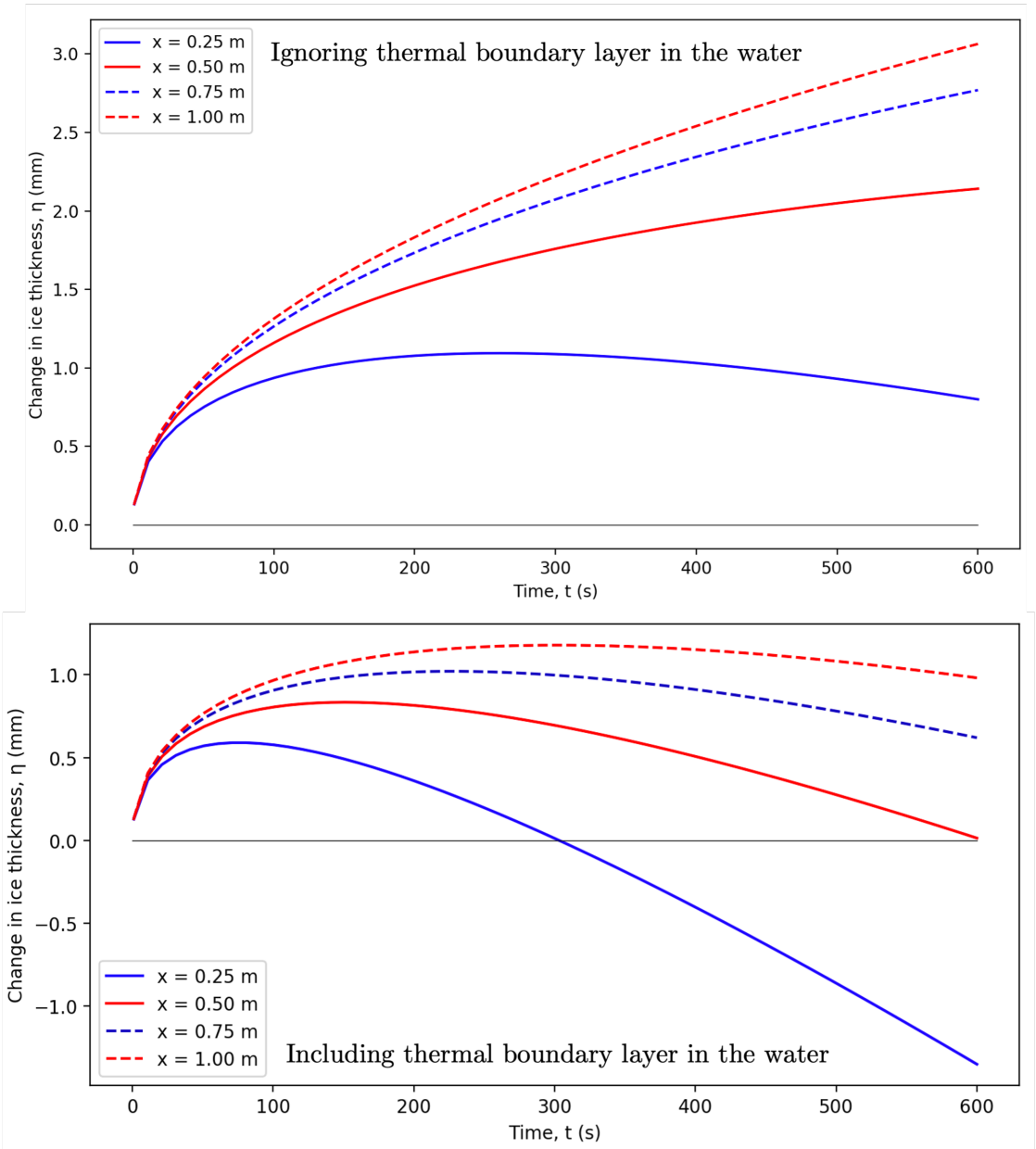

Figure 14: Ice thickness against time at several values of x; ignoring the thermal boundary layer in the water (top) and including it (bottom), for $T_{w0} = 274$ K.

Figure 14 shows the change in ice thickness with time at four positions along the slope, for both models. The profiles mimic that of Figure 9: initially, a very rapid rate of ice growth, then the rate of growth slowing, followed by melting. Melting begins at the maximum point of each curve, e.g. at about $t = 250$ s for $x = 0.25$ m for the upper graph in Figure 14. As expected, closer to the channel inlet, melting occurs sooner. If the timescale were extended, melting would eventually occur at all positions (but far down the channel, this would take a *very* long time).

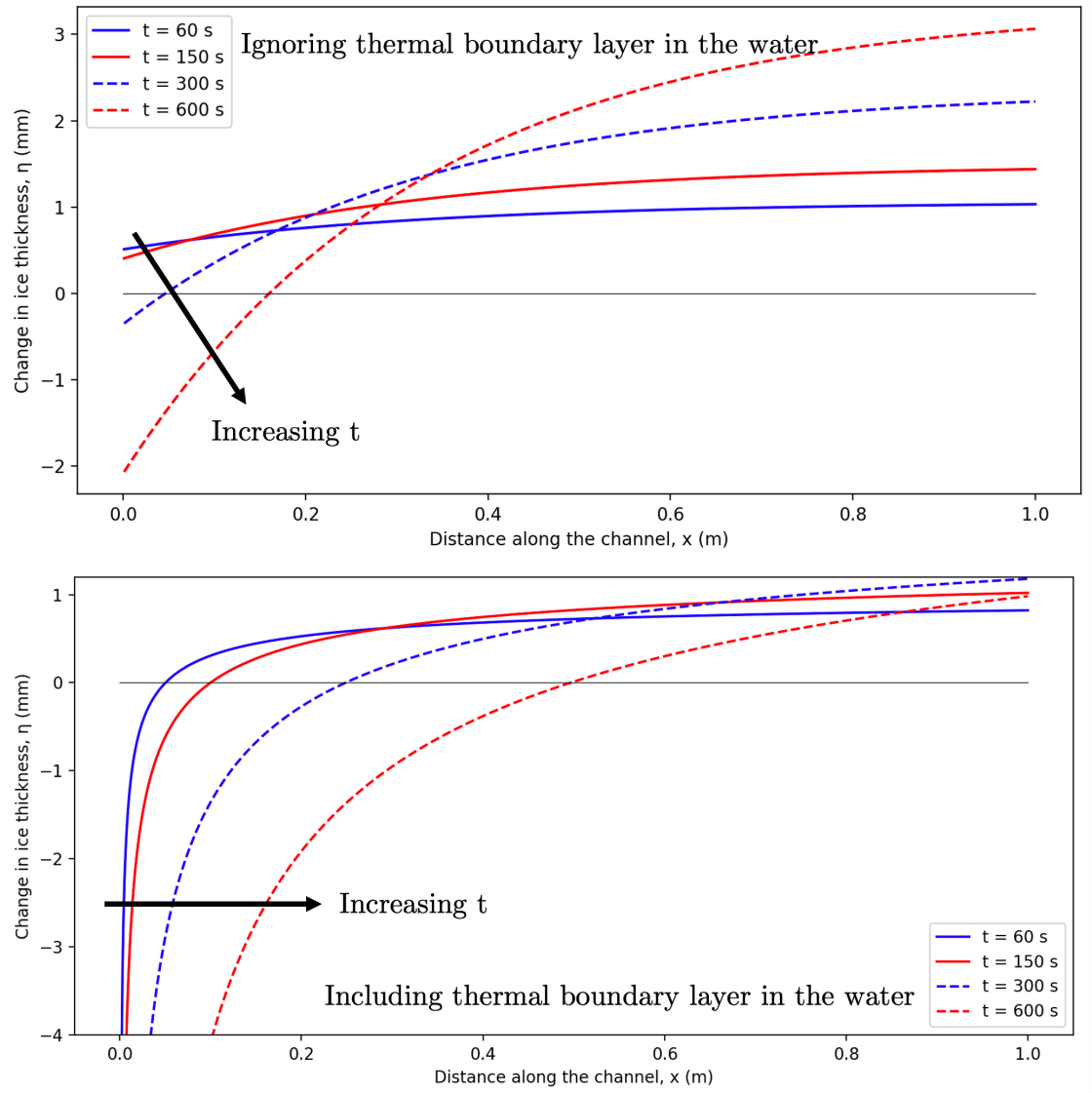

Figure 15: Ice thickness against x at t=60, 150, 300 and 600 s (i.e. snapshots of the ice profile at several points in time); ignoring the thermal boundary layer in the water (top) and including it (bottom), for $T_{w0} = 274$ K.

Figure 15 shows the predicted ice profiles (the change in ice thickness with x) after 1 minute, 2.5 minutes, 5 minutes, and 10 minutes. Initially, there is freezing everywhere due to H_1 tending to infinity (except at the very beginning of the channel, for the boundary layer case, because at $x = 0$ the boundary layer has zero thickness so H_2 is also very large). With increasing time, the ice begins to melt, first at the channel inlet where H_2 is largest (which means that H_2 exceeds H_1 sooner). As time progresses, there is more melting near the inlet, and more freezing far from the inlet.

Figure 16 shows the predicted ice profile after 10 minutes, with and without the boundary layer. As expected, near the beginning of the channel there is a net loss of ice, and towards the end there is a net gain. With the boundary layer, the predicted loss of ice at the beginning of the channel is severe, which could pose problems for the ice volcano. This will be discussed in greater detail in the following section.

The boundary layer model is much more pessimistic in outcome – it predicts less freezing

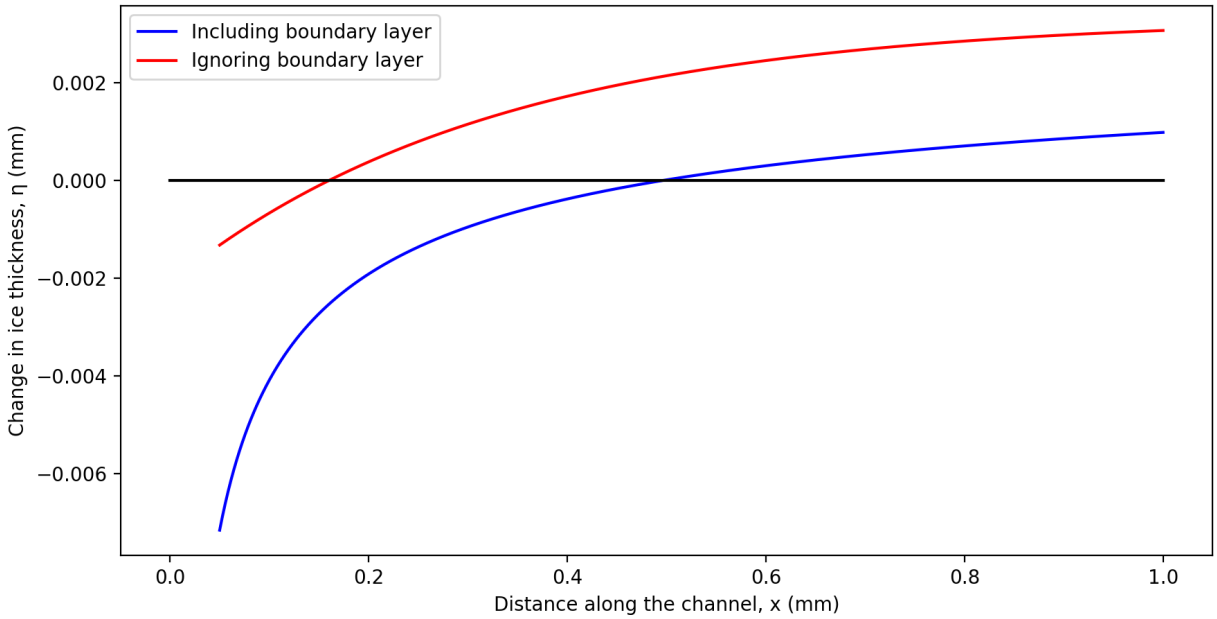

Figure 16: Ice thickness against x at $t = 600$s (i.e. the ice profile after 10 minutes); ignoring the thermal boundary layer in the water (red) and including it (blue), for $T_{w0} = 274$ K.

and more melting. This is due to it having a larger value for H_2 for the parameters used (for a different substance, this may be different). It is also worth noting that the boundary layer model is only valid until the boundary layer reaches the full depth of the film. The point at which this occurs depends on d, v and α_w. For the parameters used to create these graphs, the boundary layer should reach the full depth around $x = 0.6$ m.

2.4 Implications for the ice volcano

How is this analysis relevant for the ice volcano? The graphs presented in the previous sections have focused on short timescales (∼10 minutes) and short channel lengths (∼1 m). The analysis could simply be extended to a larger scale. Suppose we have an ice volcano of 10 m radius in operation from December to February, with water at its freezing temperature. Using the parameters specified at the beginning of this chapter, about 0.4 m of ice would be created over these three months. This is far from the necessary 3 m as set out in the introduction. If the water is initially 1°C above its freezing temperature, approximately the same amount of ice is formed from 1.5 m down the channel onwards – but at $x = 0$, there is 58 m of melting (see Figure 17), an extremely discouraging outcome. But are these results reasonable?

One of the initial assumptions for this model was to neglect radiative and convective heat fluxes from the water to the atmosphere. In his paper, Siromani predicted that radiation would account for a heat flux of 63.9 W/m^2, and convection 205 W/m^2. In comparison, using this model with the specified parameters, after 1 minute the conductive heat flux H_1 is 2680 W/m^2 – over an order of magnitude larger – so neglecting heat loss to the atmosphere is a valid assumption. However, after an hour and a half (a negligible proportion of three months), the conductive heat flux has dropped to 283 W/m^2 in the model and heat transfer to the atmosphere is now of a comparable magnitude. After three months, conductive heat flux in the model is just 7 W/m^2 and is greatly exceeded by heat transfer to the atmosphere. This indicates that heat transfer to the atmosphere is not negligible over longer timescales,

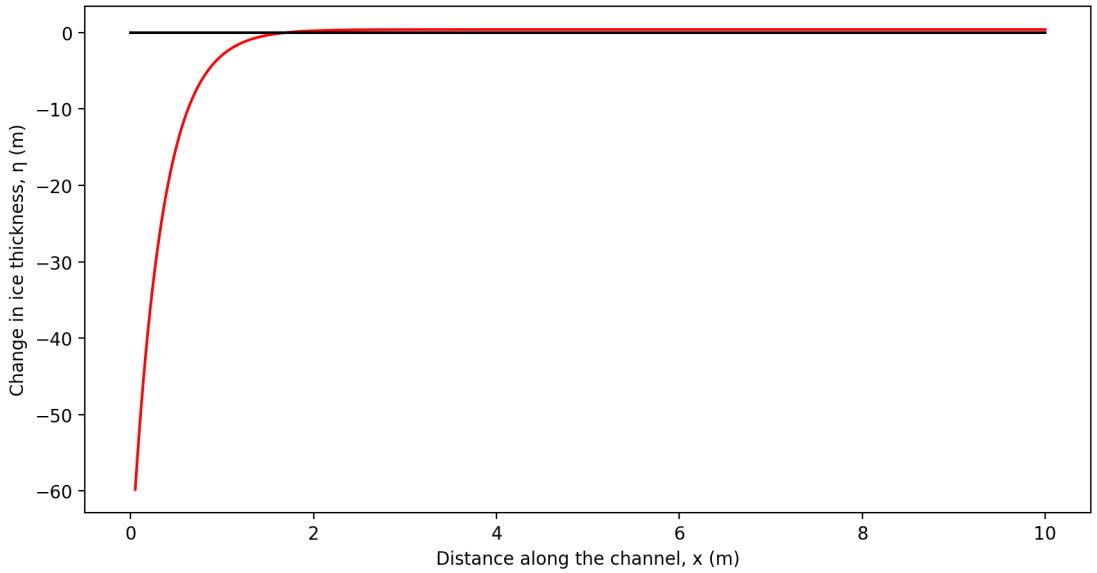

Figure 17: Ice profile for a channel of length 10 m after three months with fresh water 1°C above its freezing temperature. Around 0.4 m of ice is accumulated over the latter portion of the channel, and 58 m of melting is seen at $x = 0$, for $T_{w0} = 274$ K.

and the assumption fails in the ice volcano context.

For water 1°C above its freezing temperature, the convective heat loss to the ice, H_2, is 2757 W/m^2 – again more than an order of magnitude larger than heat transfer to the atmosphere. Unlike H_1, which decreases with time, this remains true over all timescales, since H_2 has no time-dependence. This implies that heat transfer to the atmosphere may be neglected for the case of warmer water. However, from Figure 12, it is apparent that water at 1°C cools to approximately 0°C within 2 metres, at which point the convective heat loss to the ice will be negligible (and heat loss to the atmosphere is again significant), so the approximation fails further down the channel.

The warmer the water, the higher the convective heat loss to the ice, and the more negligible the heat transfer to the atmosphere. Yet, it was stated that the 'no moving interface' approximation was only valid for water just above its freezing temperature, so that the melting distance was much smaller than the characteristic distance propagated by the temperature signal. As such, there is only a small margin of 'acceptable' temperatures.

Consolidating these order of magnitude calculations, the theoretical model analysed here is expected to be valid:

- over short timescales $t \sim 10$ minutes (which, in the context of an ice volcano left in the Arctic for 3 months, is *very* short); or
- near the beginning of the channel $x \sim 2$ m, for water entering above its freezing temperature $T_{w0} \sim 1$–3°C.

Over long timescales and far from the channel inlet, the model is a poor approximation but a conservative one, since heat transfer to the atmosphere becomes a significant contributor to freezing but is being neglected. For short timescales and near the channel inlet, the model is valid, and conservative when there is net melting, due to the 'no moving interface' assumption. This suggests that the 58 m of melting predicted at $x = 0$ is an overestimate, but not a substantial one (particularly when considering the additional problem of physical

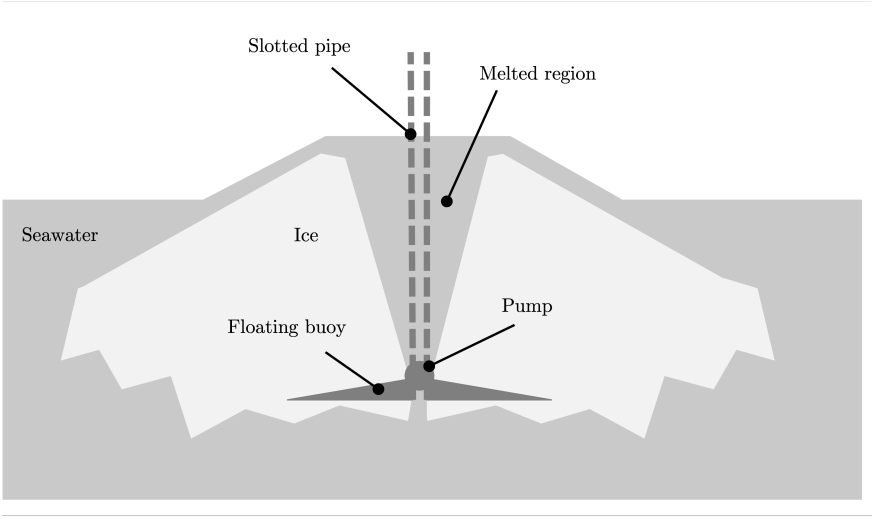

Figure 18: Situation where water enters above the melting temperature of ice. Ice is eroded around the pipe, forming a doughnut shape.

erosion). This poses an issue for the ice volcano. Around the pipe, the ice would be worn away, creating a puddle that could eventually melt through the full depth of the ice, creating more of a doughnut than a cone. Figure 18 illustrates this outcome. This is clearly not feasible. Solutions could include:

- Only operating the ice volcano when the seawater is already at its freezing temperature – but this could be very limiting and lead to low utilisation.
- Before the ice is completely eroded, pause the flow and allow the puddle around the slotted pipe to freeze, rebuilding the ice volcano to its original cone shape – but this would require very careful monitoring, to know when to pause the flow; and product design, so that the pipe and pump would not be freeze up and become blocked.
- Replacing the slotted pipe in the original design with a solid pipe, so that the water must flow over and down the whole length of the pipe before reaching the ice. It would then be exposed to the cold Arctic atmosphere and hopefully cool to its freezing temperature before reaching the ice.

2.4.1 Effects of seawater

The ice volcano will use seawater, at a salinity of approximately 32 psu, rather than fresh water. The unit used here is the *practical salinity unit* – 32 psu is equivalent to 32 g/kg, or 3.2 wt%NaCl. The presence of salt alters the thermal properties of the water. The most noticeable difference is the freezing temperature, which is –1.8°C for Arctic seawater (National Snow and Ice Data Centre, 2020 [19]).

Consider the phase diagram of Figure 19. Arctic conditions (air temperature –18°C and seawater salinity 3.2 wt%NaCl) position us in the red region, labelled 'ice + saltwater'. This region is two-phase: fresh ice and concentrated brine. The destination of this concentrated brine is of great relevance, and it is currently unknown for the ice volcano. Siromani proposed that all of the brine would be rejected into the bulk water flow and be returned to the ocean, leaving fresh, newly-formed ice with no salt pockets. Natural sea ice contains many tiny brine cells, formed when dendrites of ice grow and trap seawater inside its structure. The walls of the ice freeze and close in on the trapped water, leaving a small, very concentrated

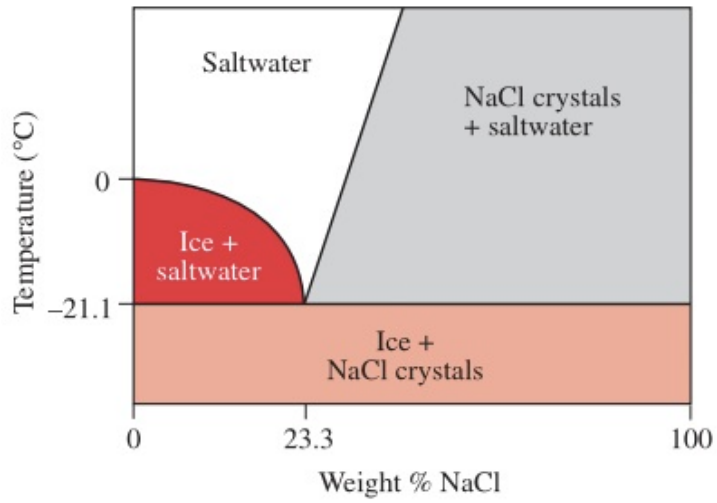

Figure 19: Phase diagram for salt and water (Harvard University, 2021 [23]) Arctic conditions place us in the red region labelled 'Ice + saltwater'.

droplet of brine that does not freeze (Wadhams, 2017 [25]). These droplets are typically 0.5 mm wide with a spacing of 0.6 mm. The brine cells gradually drain out of the ice via processes including brine cell migration, brine expulsion and gravity drainage. As such, the salinity of sea ice tends to decrease with its age: young ice is ∼10 psu, first-year ice ∼4-6 psu, and multi-year ice ∼1-3 psu. The low salinity of multi-year ice contributes to its mechanical strength, making it more resistant to wind, waves and other erosion. A further insight is that if the brine is not immediately rejected by the ice, as per Siromani's proposal, then the ice volcano design should allow for it to escape, so that its ice becomes harder and stronger.

It seems likely, or at least feasible, that the ice grown from seawater by an ice volcano would be less salty than the seawater itself, having rejected some brine into the bulk water flow. Suppose our ice has a salinity equivalent to young, naturally-formed ice, at 10 psu. The melting temperature of sea ice is a function of its salinity, obeying the relation

$$T_m = -\mu S$$

where $\mu = 0.054$°C, S is the salinity of the ice in psu and T_m is the melting temperature in °C (Bitz and Lipscomb, 1999 [2]), giving our ice a melting temperature of –0.54°C. This is useful. It was shown in the previous section that fresh water entering above its freezing temperature would cause substantial erosion in the region of ice around the pipe, eventually creating an 'ice doughnut'. This gives a very narrow operability range for the ice volcano in terms of the water temperature – it must be very close to 0°C (the minimum temperature at which fresh water can exist). However, for our ice, the water may enter between –1.8°C (the freezing temperature of Arctic seawater, and therefore the minimum temperature at which it can exist) and –0.54°C (the melting temperature of our ice) before causing substantial erosion. Although the required temperatures are lower, this is a much larger operability range and makes an ice volcano more feasible for regions with variable ocean temperatures.

Without knowing the exact destination of the salt, it is meaningless to try and repeat the calculations of the previous sections for seawater. However, it would make a useful extension to this project.

2.5 Summary of theoretical results

The key results from this section are summarised below.

- No matter the inlet water temperature, the first response of the system is freezing at a rate that initially tends towards infinity, due to the temperature profile in the ice tending to a step function.
- The interface between ice and fresh water is always at the freezing temperature, T_f.
- The rate of ice formation ($\frac{\partial \eta}{\partial t}$) is proportional to the difference between the conductive heat flux in the ice, away from the interface (H_1) and the convective heat flux from the water to the ice (H_2).
- If water enters the channel at its freezing temperature, T_f, $H_2 = 0$, and the ice grows uniformly in x, at a rate proportional to $1/\sqrt{t}$. This means that the ice continues to thicken for all t, but at a constantly slowing rate.
- H_1 is independent of x but decreases with time.
- For water initially above T_f, H_2 is independent of time but decreases with x.
- If water enters the channel above T_f, the first response is freezing everywhere. Melting will later occur, soonest at the channel inlet, since H_2 is largest here. Freezing and melting can occur simultaneously, at different positions along the channel.
- If water enters the channel above T_f, the region of ice near the channel inlet will be eroded substantially, since the rate of melting is greatest here. The water must be very close to T_f for this problem to be avoided, giving a very narrow operability range of the ice volcano.
- The model fails over timescales longer than ∼10 minutes and channel lengths beyond ∼2 m, at which point it significantly underestimates the rate of freezing due to neglecting heat transfer to the atmosphere.
- If salt water is used, the freezing temperature of the water and the melting temperature of the salty ice are likely to be different. This increases the operability range of the ice volcano, but decreases the freezing temperature of the water.

Table 1 below summarises the mathematical results derived in this chapter.

T_{w0}	Moving interface	Boundary layer	$\eta(t)$
T_f	Ignored	n/a	$\frac{2c_{pi}(T_f - T_{i0})}{L\sqrt{\pi}} \sqrt{\alpha_i t}$
T_f	Included	n/a	$2\gamma\sqrt{\alpha_i t}$
$> T_f$	Ignored	Ignored	$\frac{1}{\rho_i L}\left[\frac{2\lambda_i(T_f - T_{i0})}{\sqrt{\alpha_i \pi}}\sqrt{t} - h(T_{w0} - T_f)e^{-\frac{h}{\rho_w v d c_{pw}}x}t\right]$
$> T_f$	Ignored	Included	$\frac{1}{\rho_i L}\left[\frac{2\lambda_i(T_f - T_{i0})}{\sqrt{\alpha_i \pi}}\sqrt{t} - \lambda_w\sqrt{\frac{v}{\alpha_w x}}(T_{w0} - T_f)t\right]$

Table 1: Equations describing the ice profile for standard cases and approximations.

3 Evolution of experiments

It is useful to test experimentally the theory outlined in the previous section, both for general interest and in the wider context of the implications for an ice volcano. The experiments elaborate on those conducted by Huppert (1989) [11], who used molten wax and solid Na_2CO_3 to demonstrate simultaneous melting and solidification. This chapter describes the evolution of experiments over the course of the project. Their main objectives were:

- to test a two-dimensional model of an ice volcano in Arctic conditions and investigate the feasibility of the idea;
- to substantiate the theory of the previous chapter;
- to evaluate the validity of assumptions made in the previous chapter;
- to assess the sensitivity of an ice volcano to its environment; and
- to explore physical differences when using salt water.

Where 'fresh' water is mentioned in the following sections, this refers to water from the tap, with negligible salt content, rather than distilled water. For these experiments, tap water was sourced from Cambridge City North water quality zone (Z1), which, according to the most recent water quality report (Cambridge Water, 2020 [26]), is classified as 'Hard' with a mean $CaCO_3$ content of 281.3 mg/l and sodium content of 11.23 mg/l. In contrast, the sea has a typical sodium content of 10.8 g/l – almost three orders of magnitude larger – so it is reasonable to consider this tap water as having negligible salt content.

3.1 Preliminary experiments

A household freezer was used to conduct several preliminary experiments. Their objectives were to verify the basic principle of water freezing and to identify discernible differences between the behaviour of fresh water and salt water, rather than to be the basis of any rigorous analysis.

Two 20 ml syringes were filled with fresh water and salt water of salinity 32 psu (equivalent to Arctic seawater). The syringes were positioned, within the freezer, at the top of an aluminium plate on a slight incline and slowly pushed to release the water (see Figure 20). Aluminium was chosen for its high thermal conductivity, to keep the plate temperature (and thus the boundary condition on the water) approximately uniform. The plate had been left in the freezer overnight at –18°C and the water had been refrigerated at 5°C.

Both the fresh and salt water froze onto the plate and formed ice trails soon after being released. The salt water trail was about twice as wide as that of the fresh water and had a markedly softer consistency, resembling slush. With light pressure, it could be broken up or moved around, whereas the fresh water trail was solid, firmly attached to the plate and could not be moved by hand until it had begun to melt. Figure 21 depicts a photograph with examples of such trails. Upon closer inspection, it seemed that the salty ice was characterised by many small pockets of brine enclosed in the crystalline ice structure, similar to that of natural sea ice. This suggested that Siromani's assumption – that the newly formed ice would contain no salt or brine pockets – was invalid over the timescales of these experiments. Over a longer duration, the brine cells may be able to penetrate the crystal structure and escape the ice, as seen in natural sea ice, but this was not observed here.

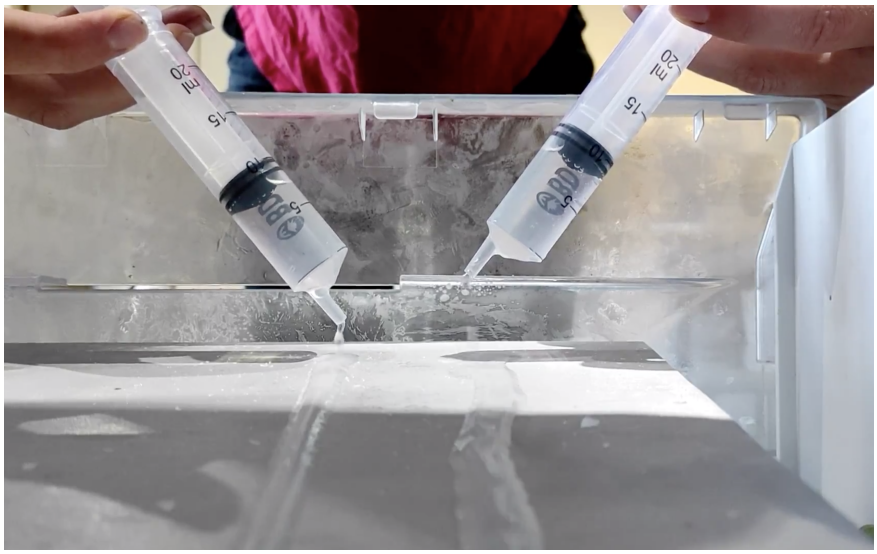

Figure 20: Syringes of fresh water (left) and salt water (right) producing trails on a cold aluminium plate in a household freezer.

Figure 21: Resulting salt water (upper) and fresh water (lower) ice trails on the aluminium plate.

The preliminary experiments were limited by their small scale and dissemblance to Arctic conditions (the freezer door had to be open, so the surrounding air was relatively warm), but, having demonstrated the principle that water would freeze on a cold slope, this laid the way for future experiments.

3.2 Development into larger-scale experiments

In order to conduct experiments on a larger scale and with better resemblance to Arctic conditions, a walk-in freezer, belonging to the kitchens of Trinity College, Cambridge, was used as a cold room. The freezer has dimensions of approximately $3 \times 1.5 \times 2$ m and maintains a temperature of –18°C, which is comparable to Arctic winter temperatures (Labe, 2022 [13]). The objectives of this series of experiments were to become familiar with working in the freezer and to refine experimental technique.

Equipment used was as follows:

- a 30 litre plastic container with an adjustable tap;
- 1.5 m of flexible rubber tubing;

- an aluminium U channel of external dimensions $44 \times 44 \times 1000$ mm and thickness 3 mm; and
- a collection container for excess water.

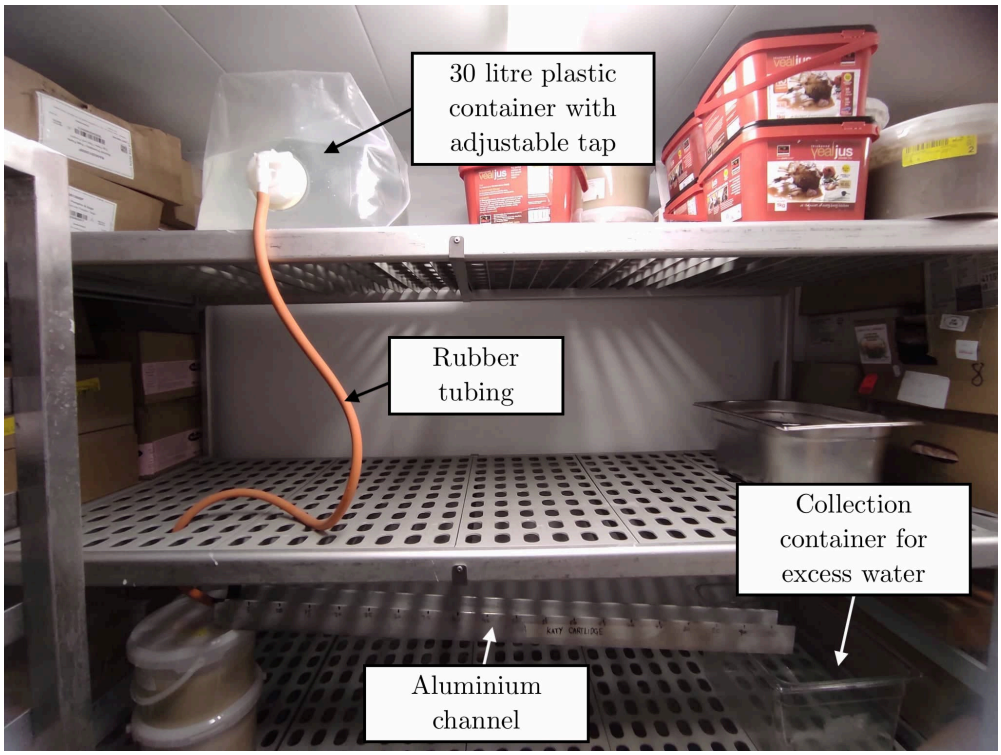

Figure 22: Experimental setup in the freezer. By adjusting the position of the tap on the plastic container, water flows down the rubber tubing and through the aluminium channel. Excess is collected in the second container.

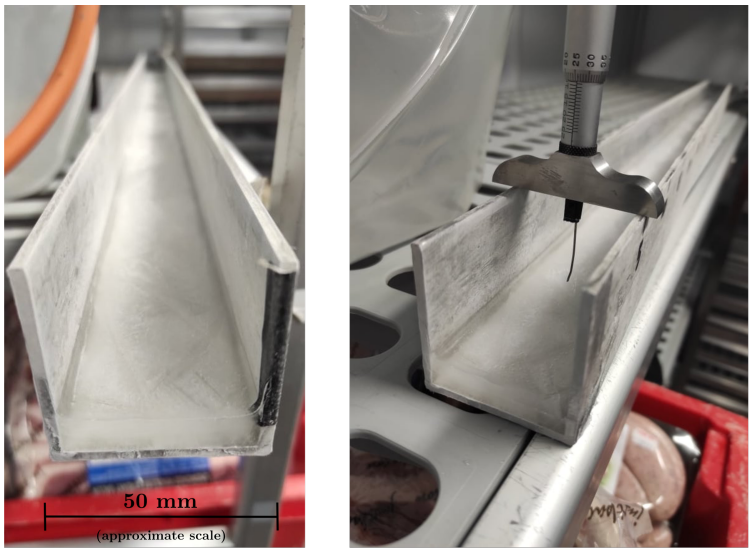

Figure 23: A layer of 'original' ice in the base of the channel (left); measuring ice thickness using a depth micrometer (right).

To compare experimental and theoretical results, the aluminium channel must be mapped to the two-dimensional ice volcano 'slice' described in the previous chapter. For this mapping to hold, behaviour must be uniform widthways in the channel.

The experimental setup was as shown in Figure 22. Prior to each experiment, all equipment was at –18°C (having been left in the freezer for some time), and a layer of 'original' ice approximately 1 cm thick was frozen in the base of the channel, using fresh water. By adjusting the tap on the plastic container, a gravity-fed flow of water (at the chosen temperature and salinity) was discharged into the channel, where it could freeze or melt existing ice. The channel had a slope of 1 in 10 (an angle of 6° to the horizontal).

Before and after each experiment, the thickness of the ice was measured at 5 cm intervals along the channel using a depth micrometer (see Figure 23). Measurements were taken at two points across the width of the channel at each location. If these differed by more than 0.5 mm, a third measurement was taken. The data was used to generate ice profiles. This type of experiment is referred to hereafter as a 'termination experiment', since data is gathered upon terminating the water flow. Measurements are generated along the entire length of the channel, but at a singular point in time (the time at which the experiment is stopped).

This series of experiments helped to establish the experimental process in the freezer, but had notable limitations:

- The tap had no markings, so it was difficult to control the flow rate between experiments.
- The water sometimes failed to fill the entire width of the channel, invalidating the two-dimensional widthways behaviour requirement.
- The aluminium base and sides imposed unrealistic boundary conditions, since aluminium has a much higher thermal conductivity than ice – effectively, the base and sides of the channel were being held at –18°C.
- It was difficult to clearly see the shape of the ice profile from above.
- The thickness of the original ice often varied by up to 2 cm along the length of the channel, affecting the flow and freezing patterns.
- The original ice was thin in comparison to the characteristic distance propagated by the temperature signal during the experiment, invalidating the theoretical assumption that the ice could be considered semi-infinite.

3.3 Termination and transient experiments

The objective of the remaining experiments was to gather useful data that could be compared with the theoretical predictions and used to evaluate the ice volcano concept. Two types were conducted: termination experiments (as mentioned above) and transient experiments. Termination experiments return data only for a singular point in time (the end of the experiment) but along the whole length of the channel. Transient experiments return data across the whole time period, but only at a singular position along the channel. The process for a transient experiment is described at the end of this section.

A pump and a new channel were acquired to offset the five limitations mentioned above. The *Watson Marlow 505S Peristaltic Pump* was used. This is a positive displacement pump whose flow rate can be varied by adjusting the angular speed of the rollers and tube diameter. For all experiments, the pump was set to 50 rpm, which was calibrated as a flow rate of 5.4 cm^3/s.

The new channel had Perspex sides and base, with a thick aluminium foundation to act as a 'coolth' reservoir. The sides were screwed to the base, which was screwed to the aluminium bar using acrylic screws, then waterproofed with silicone sealant. Perspex was chosen for its transparency, to allow the ice profile to be seen clearly; and for its low thermal conductivity, so as to minimise conduction from the ice to the sides and base of the channel, which would affect its temperature profile. A scaled SketchUp model of the new channel (not including screws) is shown in Figure 24.

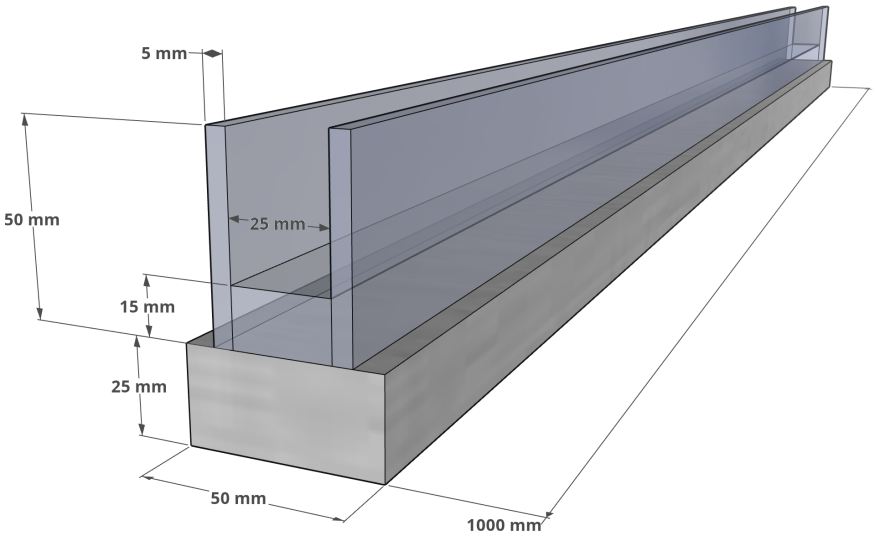

Figure 24: Scaled SketchUp model of the new channel, with an aluminium foundation and Perspex sides and base.

This channel was narrower than its predecessor, with a width of 25 mm, so that water filled the entire width of the channel at the chosen flow rate. A thicker layer of original ice was frozen in it prior to each experiment, comparable to the characteristic propagation distance of the temperature signal, $z \sim \sqrt{\alpha t}$, which is 24 mm after 8 minutes. Original ice thickness in the channel was around 20 mm, so it is only towards the end of the experiment that the semi-infinite assumption will start to fail. Prior to this, the temperature signal has not yet penetrated the ice fully, and thus is unaware that it is not semi-infinite. The original ice was smoothed before beginning each experiment using a warmed piece of aluminium that served as a *Zamboni*, to resolve the variations in original ice thickness seen in earlier experiments. The topmost layer of ice was melted and allowed to refreeze, during which time the resulting water had flowed to the lowest point. This created a more level ice surface.

Figure 25 shows the updated setup for this series of experiments, with the new channel and pump replacing the old channel and plastic container. For the transient experiments, the method was as follows. During the 'Zamboni' process, a small amount of red food colouring was dropped onto the melted ice to visually highlight the position of the ice surface. A tape measure was then attached alongside the channel, and vertical scratches were made in the Perspex sides to identify particular locations. The channel was photographed at set time intervals throughout the experiment. The photos were taken with the Redmi Note 9 phone camera at a resolution of 16 MP (see Figure 26 for examples). The photographs were analysed in *ImageJ 1.x*, an image processing program developed in the public domain, which allows the user to measure distances from pictures. The scale was calibrated manually for each image from the tape measure attached to the channel, then the ice thickness measured and results consolidated into transient ice profiles.

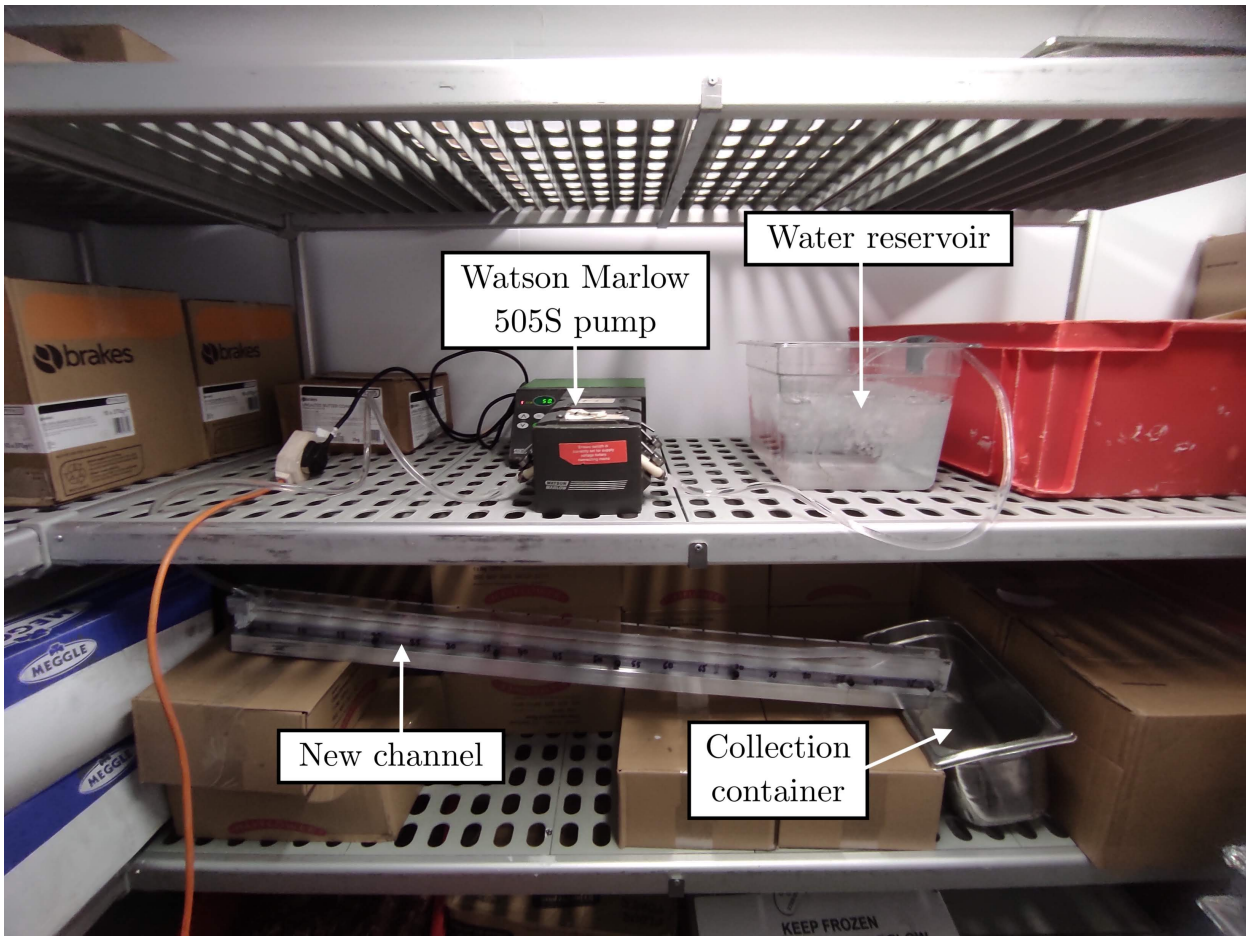

Figure 25: Experimental set-up for termination and transient experiments. Note the updated channel, and that the water reservoir and *Watson Marlow* pump have replaced the 30 litre plastic container with an adjustable tap.

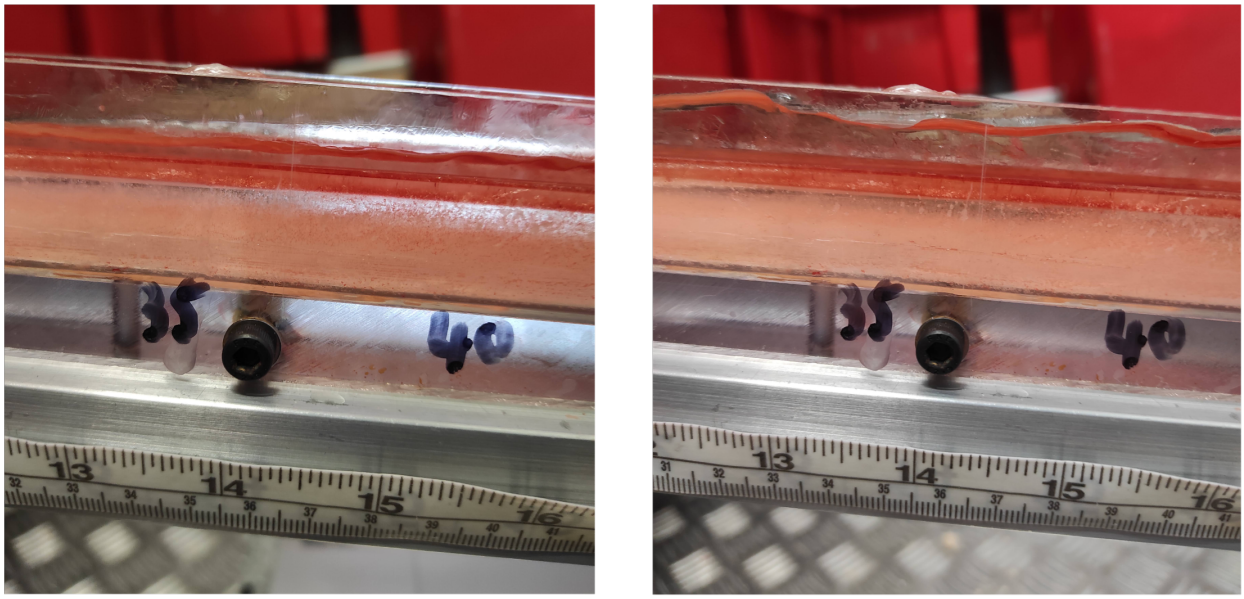

Figure 26: Examples of photographs used to collect transient data; after 32 seconds (left) and 480 seconds (right).

4 Discussion

To compare the theoretical and experimental results, the Perspex channel must be mapped to the two-dimensional 'slice' model. The water enters the channel at $x = 0$ and the end is at $x = 1$ m. The surface of the original ice is $z = 0$. Since a three-dimensional channel is being mapped onto a two-dimensional model, for the mapping to be valid, behaviour in the channel must be uniform across its width (in what would be the y-direction), i.e. uniform melting and freezing rates, uniform velocity, uniform film depth, etc.

Table 2 summarises the experiments whose results are discussed in the following sections. Each has been given a reference letter A–H.

Termination experiments			Transient experiments		
Reference	Salinity (psu)	Temp. (°C)	Reference	Salinity (psu)	Temp. (°C)
A	0	0	E	0	0
B	32±2	–1.8	F	32±2	–1.8
C	0	4±0.5	G	0	2±0.5
D	32±2	1±0.5	H	32±2	1±0.5

Table 2: Summary of experiments, by water salinity and inlet water temperature.

The thickness of the thermal boundary layer in the water scales with $\delta(x) \sim \sqrt{\alpha_w x/v}$. For the parameters of these experiments, boundary layer thickness should match film depth approximately 0.6 m from the channel inlet. Including the thermal boundary layer in calculations is not a valid approximation beyond this point.

The theoretical model was based on fresh water and ice, which have freezing and melting temperatures that are equivalent and constant (at 0°C). However, for salt water and ice, these temperatures are a function of its salinity – the higher the salinity, the lower the freezing and melting points, and vice versa. Mathematical analysis for salt water is beyond the scope of this project, so the fresh water theory has been adapted for comparison with the salt water experimental results.

The salt water used in experiments B, D, F, and H had a freezing temperature of –1.8°C. The ice grown from this salt water has an unknown salinity, but the most optimistic prediction is that it is completely fresh and therefore has a melting temperature of 0°C. The original ice in the channel was grown from fresh water, so certainly has a melting temperature of 0°C. This places two constraints on the salt water results: the water will freeze at a minimum of –1.8°C, and the ice will melt at a maximum of 0°C. For the case where water enters at its freezing temperature, the only adjustment to the mathematical model was to set T_f to –1.8°C (since only freezing occurs). For the case when water enters above its freezing temperature, two theoretical predictions are shown on the graphs: a lower bound governing the freezing of the water (T_f set to –1.8°C) and an upper bound governing the melting of the ice (T_f set to 0°C). The experimental results should lie between these two lines. This concerns Figures 30 and 36. In reality, the presence of salt will affect many of the properties of water and ice, such as the latent heat of fusion, thermal conductivity, density and specific heat capacity (Wadhams, 2000 [24]). All of these are a function of the salinity, which was unknown in these experiments (apart from the inlet water salinity at 32 psu)

due to uncertainty in the final destination of the salt. The parameters for fresh water were therefore used in all mathematical analysis.

4.1 A note on uncertainties

The salt water was produced by dissolving 165 g of table salt in 5 litres of tap water, giving a nominal salinity of 32 psu. The absolute uncertainties were ±100 ml for the water and ±5 g for the salt, giving an uncertainty of ±2 psu.

The water inlet temperature was measured using a digital probe thermometer, correct to ±0.05°C. However, during the experiment, the water cooled by approximately 1°C (since it was also sitting in the freezer). The overall uncertainty is therefore ±0.5°C. The water temperatures in experiments A, B, E, and F do not have this uncertainty, as the water was initially at its freezing point, so could not cool further.

The depth micrometer used in the termination experiments had a precision of ±0.05 mm, though an experimental uncertainty in η of ±0.5 mm is more reasonable, to account for human error and the compliance of the ice. The transient experiments measured the ice thickness from photographs with a resolution of 16 MP. 10 mm in the photograph spanned an average of 480 pixels, with the interface position definable within an average of 50 pixels, also giving an uncertainty of ±0.5 mm in η. The uncertainties are represented by vertical error bars on the graphs.

Table 3 summarises the value of parameters used in the mathematical models. Parameters marked with an asterisk (*) were measured or calculated (see paragraphs below), those without are known values.

Parameter	Value	Unit	Parameter	Value	Unit
α_i	1.18×10^{-6}	m^2/s	c_{pw}	2.09	kJ/kgK
α_w	0.132×10^{-6}	m^2/s	h*	2760±920	W/m^2K
λ_i	2.22	W/mK	T_f	0	°C
ρ_i	916	kg/m^3	T_{i0}*	-18±0.5	°C
ρ_w	1000	kg/m^3	v*	0.6±0.2	m/s
c_{pi}	4.20	kJ/kgK	d*	0.36±0.18	m/s

Table 3: Summary of values used for key parameters in the following result comparisons.

It was assumed that the initial ice temperature would be the same as that of the freezer, at –18°C, since the channel and original ice were left there for at least 24 hours prior to each experiment. This temperature was displayed outside of the freezer to the nearest 1°C, giving an absolute uncertainty of ±0.5°C in T_{i0}.

By calibrating the *Watson Marlow* pump, the volumetric flow rate into the channel, Q, was measured as 5.4 ml/s. The flow velocity, v, was calculated by dropping a small quantity of food dye into the water and measuring the time it took to travel the length of the channel. This gave a result of 0.6 m/s. The human error associated with this timing is 0.5 s, giving an absolute uncertainty of ± 0.2 m/s for the 1 m channel. The width of the channel, b, was measured as 25 mm. The film depth, d, is found using the relation $d = Q/vb$, giving a value of 0.36 mm. Due to the uncertainty associated with v, d has a percentage uncertainty of 50%.

It has been shown that the overall heat transfer coefficient between water and ice varies according to the relation $h = 4594.8v$ (Nan Li et al., 2016 [14]), giving $h = 2760 \pm 920$ W/m^{2}K for the measured experimental velocity.

4.2 Termination experiments

This section compares the outcomes of the four termination experiments (A–D) with theoretical predictions from the models of the previous chapter. For all graphs in this section, the y-axis represents the change in ice thickness (η) and the x-axis represents distance along the channel (x).

We begin with a brief summary of the method for termination experiments. The thickness of the original ice in the channel was measured at 20 positions along its length. Water was then pumped through the channel where it could freeze or melt existing ice; after some time the pump was switched off and excess water allowed to flow out. The ice thickness was then measured again to give an updated value at the 20 positions (each one representing an average across the width of the channel). The difference from before to after was plotted. As such, the termination experiments return data along the whole channel, but at a singular point in time – a snapshot of the ice profile as it was at that moment.

4.2.1 Water initially at its freezing temperature

For water initially at the freezing temperature, ice accumulation should be uniform, i.e. independent of x, and there should be no melting. For a termination experiment, this means that the theoretical prediction is a horizontal line at the relevant value. The moving interface equation $\eta = 2\gamma\sqrt{\alpha_i t}$ is used to predict the change in ice thickness.

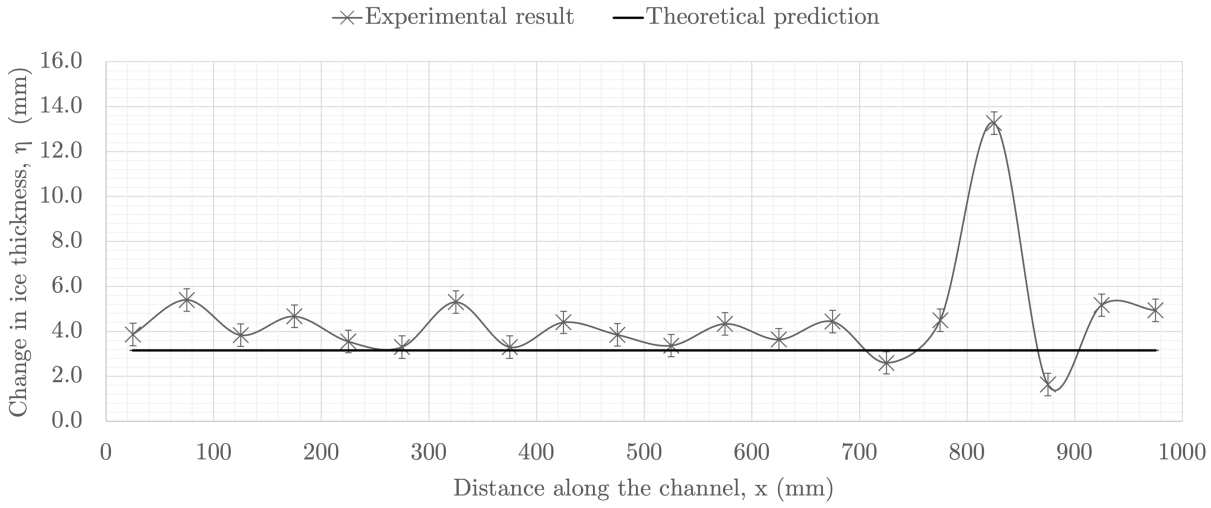

Figure 27: Experiment A: 0°C, fresh water, 10 minutes. Termination results compared to theoretical prediction of 3.16 mm (including the moving interface) with vertical error bars of ±0.5 mm.

Experiment A (Figure 27) used fresh water at 0°C and had a duration of 10 minutes, giving a predicted build-up of 3.16 mm. The anomalous data point was the result of a large lump in the original ice, which altered the surrounding flow patterns and caused an excessive build-up of ice just past 0.8 m. Ignoring this outlier, the average experimental build-up was reasonably uniform along the channel, though slightly higher than the prediction at

4.1 mm. This is promising for the ice volcano, suggesting that the ice formation technique would be successful. Uniform ice build-up is also useful, because it indicates that the ice volcano would be homogeneous and equally effective over a wide area of ocean.

Several factors may have contributed to the discrepancy in ice build-up between the predicted and experimental values. Firstly, the model ignores evaporative, convective and radiative heat transfer to the air. For water at its freezing temperature, any heat loss triggers a phase change, so contributions to ice build-up from heat loss to the atmosphere can be added linearly to contributions from conduction and convection to the ice. Siromani estimated that heat fluxes to the atmosphere from convection and radiation would total 269 W/m^2, and evaporation below 10 W/m^2. These fluxes would create 0.5 mm of unaccounted-for freezing. The discrepancy could also be explained by some newly-formed ice crystals floating on the surface of the water and being carried downstream until they become stuck. This could invalidate the moving interface approximation, if ice is not being accumulated on the base of the flow (and causing the interface to move) but rather on the top. Without this approximation, a further 0.2 mm of ice would be predicted. Finally, the presence of ripples in the ice profile could have contributed to inconsistencies between the model and the experimental results. This is discussed in detail at the end of this chapter. The remaining excess freezing could be the result of inconsistencies between the model and the experimental setup – in particular, the semi-infinite ice assumption.

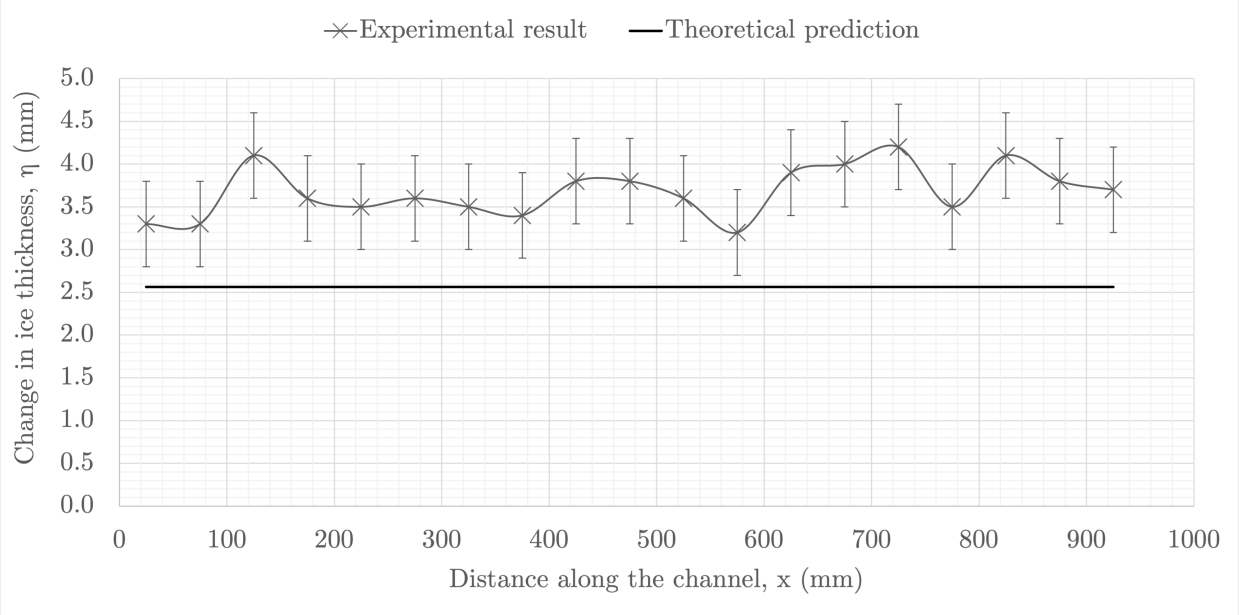

Figure 28: Experiment B: –1.8°C, 32 psu, 10 minutes. Termination results compared to fresh water theoretical prediction of 2.56 mm (including moving interface, $T_f = -1.8$°C) with vertical error bars of ±0.5 mm.

Experiment B (Figure 28) was the equivalent of Experiment A, but using salt water. The water was at –1.8°C (its freezing temperature) and the experiment lasted 8 minutes, giving a predicted build-up of 2.56 mm when T_f is set to –1.8°C in the model. Once again, ice accumulation exceeded its predicted value, with an average build-up of 3.7 mm. However, the profile was reasonably uniform in x.

Heat loss to the atmosphere, floating ice crystals, and the presence of ripples were again probable causes of the disparity between experimental results and theoretical prediction.

However, the percentage difference is much greater for these results than for the fresh water, so there are likely other factors responsible. One possibility is the presence of the salt. The resulting 'ice' from this experiment appeared to in fact be a two-phase mixture of pure ice and concentrated brine. It had a soft, slushy consistency and visibly contained unfrozen liquid, unlike the fresh water ice of Experiment A, which was firm and solid. This is known as a 'mushy layer' and is a phenomenon exhibited in natural sea ice (Feltham et al., 2006 [8]). A mushy layer obeys governing equations different to those considered in this project, so it is understandable that the model is a weaker fit for salt water.

4.2.2 Water initially above its freezing temperature

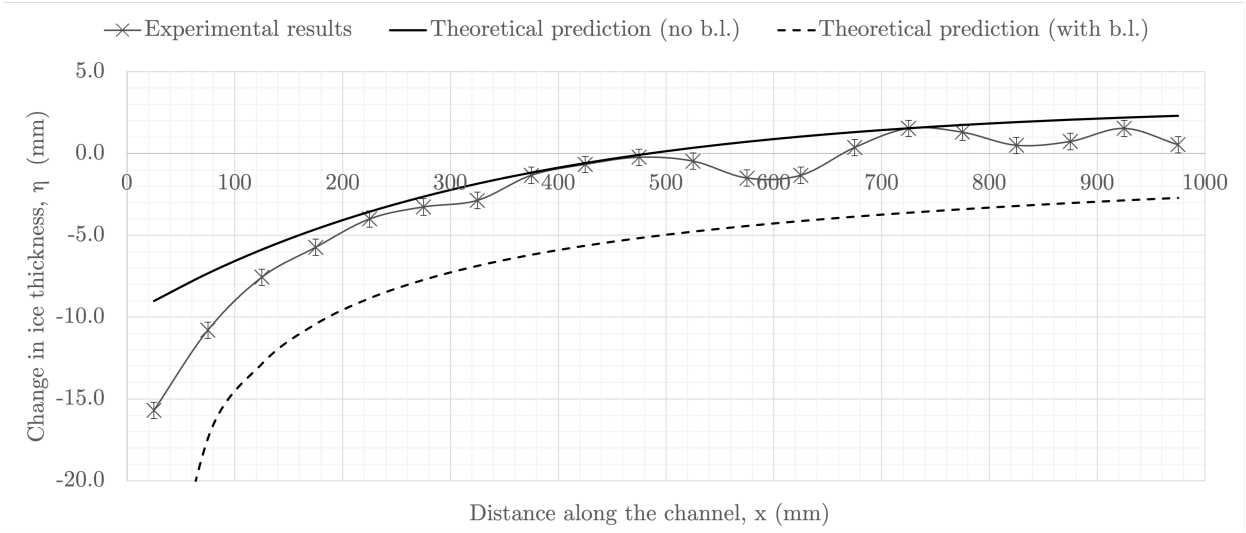

Figure 29: Experiment C: 3°C, fresh water, 8 minutes. Termination results compared with two theoretical predictions: including the boundary layer (dashed line), and ignoring the boundary layer (solid line). Vertical error bars of ±0.5 mm.

For water initially above the freezing temperature, ice accumulation is a function of t and x. For a termination experiment, we expect a net loss of ice at the beginning of the channel (where H_2 is large and quickly exceeds H_1), followed by build-up further down (where H_2 is smaller). This was indeed the case for Experiment C (Figure 29), which used fresh water at 3°C and had a duration of 8 minutes. There was substantial ice loss near the channel inlet, with a change in ice thickness that far exceeded the quantity of ice gained further down the channel. This could be problematic for an ice volcano, suggesting the region of ice around the pipe would be quickly eroded. This would lead to the 'ice doughnut' outcome considered in Section 2.4 and render the ice volcano ineffective. This suggests that the ice volcano could be highly sensitive to its environment, specifically to water above 0°C. To prevent this problem, the inlet water temperature must be at (or very close to) its freezing temperature – a narrow range of operation.

Predictions both including the boundary layer (dashed line) and ignoring it (solid line) are shown in Figure 29. Let us evaluate these two models. The model ignoring the boundary layer gives a generally good fit all along the channel, although it underestimates the melting at the beginning and overestimates the freezing at the end. The model including the boundary layer wholly underestimates the freezing, lying below the experimental line along the whole channel.

For water above its freezing temperature, the 'no moving interface' approximation was used

in the theoretical model. In the case of net melting, this was expected to be a conservative estimate – i.e. the prediction would overestimate the melting seen in the experiments – because the temperature gradient in the ice is steeper in reality than it is in the model. In the case of net freezing, the approximation was expected to overestimate the quantity of ice build-up, because the temperature gradient is shallower in reality than it is in the model. When the boundary layer is included (the dashed line in Figure 29), the melting is indeed overestimated, and when the boundary layer is ignored (the solid line in Figure 29), the freezing is slightly overestimated.

The 'no moving interface' assumption cannot be the only reason for the discrepancy between the boundary layer prediction and the experimental results. When the net change in ice thickness is zero, the no moving interface assumption should have no effect, but the dashed line is below the experimental line along the whole channel, even when the experimental result is zero net change (around $x = 0.5$ m). However, the solid line almost perfectly matches the experimental results at $x = 0.5$ m. This suggests that ignoring the boundary layer is certainly the better model by this point (and continues to be the better model beyond that point).

It seems likely that including the boundary layer gives the better model at the very beginning of the channel, but that the change in ice thickness due to melting is overestimated due to the 'no moving interface' approximation. After a short distance, ignoring the boundary layer gives the more accurate model. Beyond 0.5 m, where the result is net freezing, ice build-up is slightly overestimated due to the 'no moving interface' approximation. This approximation has a much larger effect at the beginning of the channel compared to the end, because the distance between $z = 0$ (the assumed interface) and the true interface is largest there.

From Figure 29, the solid line seems to become the better model around 0.15 m from the channel inlet, much sooner than the 0.6 m predicted in the introduction to this chapter. This disparity is most likely due to neglecting heat loss to the atmosphere – the air in the freezer was –18°C, so the water was being cooled from above as well as from below. This means that the temperature of the water outside the boundary layer would not remain T_{w0}, as assumed in the model, but would decrease with exposure to the air.

Overall, the model ignoring the boundary layer was the better one for these experiments, so is the only one included on the following salt water graph in Figure 30. This is mainly to avoid over-complicating the graph, since there are already two theoretical prediction lines on it to represent the different freezing and melting temperatures of salt water and salty ice.

Experiment D (Figure 30) used salt water at 1°C and had a duration of 8 minutes. Two predictions are shown in Figure 30, one representing the water freezing (solid line), where T_f was set to –1.8°C, and one representing the ice melting (dashed line), where T_f was set to 0°C. This was to account for the fact that freezing and melting take place at different temperatures. The solid line forms a lower bound, whilst the dashed line forms an upper bound. In the first half of the channel, the dashed line appears to be a better fit, suggesting that melting is the governing process. In the second half, the solid line is more accurate, indicating that freezing governs. This makes sense: there is net ice loss close to the beginning of the channel, so melting has been the dominant behaviour at this point, and net ice gain towards the end of the channel, so here, freezing has been the dominant behaviour. As in Experiment C, freezing is slightly overestimated by the model at the end of the channel due

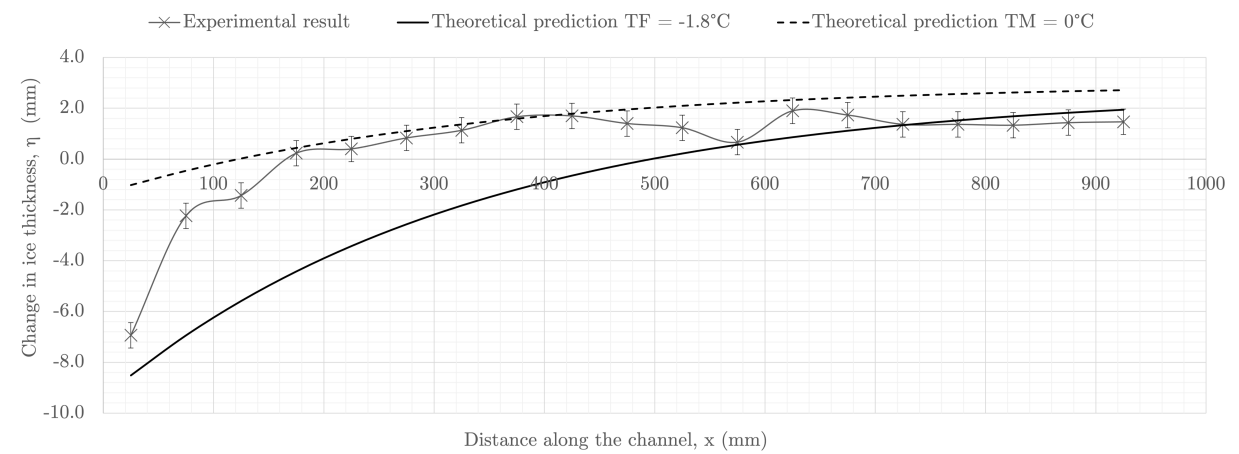

Figure 30: Experiment D: 1°C, 32 psu, 8 minutes. Termination results compared to two theoretical predictions: $T_f = 0$°C (dashed) and $T_f = -1.8$°C (solid). Both ignoring boundary layer. Vertical error bars of ±0.5 mm.

to the 'no moving interface' assumption.

In Experiment D, the salt water entered the channel at 1°C, approximately 3°C above its freezing temperature. Yet, less than half as much melting was seen at the channel inlet in Experiment D compared to Experiment C, which used fresh water at 3°C (also 3°C above its freezing temperature). This is evidence that the ice grown from salt water has a lower salinity than the salt water itself, meaning that the melting temperature of the salty ice is higher than the freezing temperature of the salt water. Although the water entered the channel 3°C above its *freezing temperature*, it was *less than* 3°C above the ice's *melting temperature*, so did not cause as much melting as in Experiment C. This has positive implications for the ice volcano – rather than water having to be at its freezing temperature to avoid significant erosion around the pipe, the water may be between its freezing temperature and the melting temperature of the ice. This implies there is a greater range of seawater temperature for which the ice volcano would be effective.

The ice produced in Experiment D had a slightly different texture to the 'mushy layer' of Experiment B. Although it still visibly contained pockets of brine, there were fewer of them, and the ice was stronger and harder. It held its shape when picked up and could be snapped in a similar manner to chocolate. This phenomenon is presumably due to the difference in inlet water temperature, that being the only notable distinction between the experiments. Perhaps the two phases of ice and brine have time to physically separate for water initially above its freezing temperature, which must cool before it can solidify, rejecting brine into the flow and out of the channel. On the other hand, for water at the freezing temperature, any heat loss will immediately trigger a change in phase, which may have led to more brine becoming trapped by the ice and creating the mushy layer. A lower brine content in ice grown from water initially above its freezing temperature may also explain why the theoretical prediction is a better fit for Experiment D than B. It would be useful to conduct salinity tests on ice grown from salt water both initially at and above its freezing temperature to check this hypothesis.

For both fresh and salt water, the theoretical predictions seem to give a better fit to the experimental results for water initially above its freezing temperature than for water at its freezing temperature. This could be because the dominating heat flux in the latter

case is conduction, which, by the end of the experiment, is comparable to heat fluxes to the atmosphere (that are neglected by the model). However, for water initially above its freezing temperature, the dominating heat flux is convection, which far exceeds heat fluxes to the atmosphere throughout the whole experiment.

4.3 Transient experiments

This section will compare the outcomes of the four transient experiments (E–H) with theoretical predictions from the models of the previous chapter. For all graphs in this section, the y-axis represents the change in ice thickness (η) and the x-axis represents time (t).

We begin with a brief summary of the method for transient experiments. A small amount of red food colouring was frozen into the original ice to visually highlight the position of its upper surface. As before, water was pumped through the channel for several minutes. Simultaneously, photographs were taken of a marked position at set time intervals. Image processing software was used to determine the change in ice thickness for each picture. Transient experiments return data across the whole time period, but only at a singular position.

4.3.1 Water initially at its freezing temperature

For a transient experiment involving water at its freezing temperature, η should scale with $\sqrt{t}$. To check this dependence, graphs of $\log \eta$ against $\log(t)$ are plotted with a linear line of best fit, which should have a gradient of 0.5 if the relation is correct.

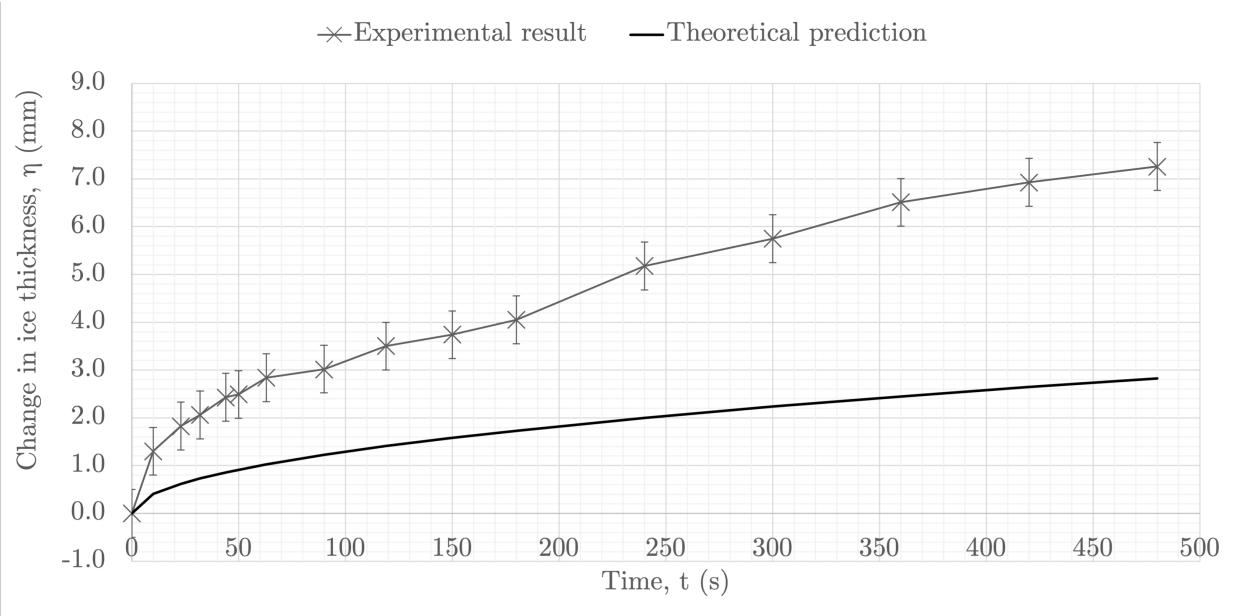

Figure 31: Experiment E: 0°C, fresh water, $x = 0.35$ m. Transient results compared to theoretical prediction (including the moving interface) with vertical error bars of ± 0.5 mm.

Experiment E (Figure 31) used fresh water at 0°C. Photographs were taken 0.35 m down the channel over a period of 8 minutes. The experimental results exceed the predicted ice growth quite dramatically; it is off by a factor of 3. Furthermore, the build-up exceeds that of Experiment A (4.1 mm) within 3 minutes, despite Experiment A having a duration of 10 minutes. This is likely a fault of the transient experimental method. Whereas in the

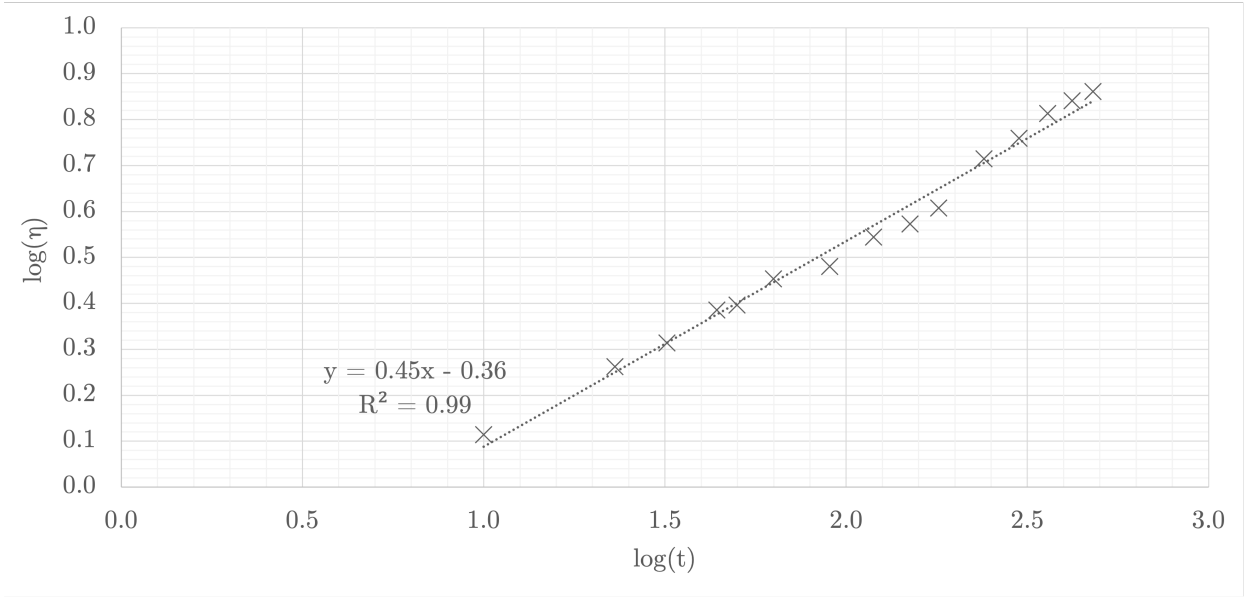

Figure 32: Log-log graph of Experiment E results, with line of best fit $\log \eta = 0.45 \log t - 0.36$ and coefficient of determination $R^2 = 0.99$.

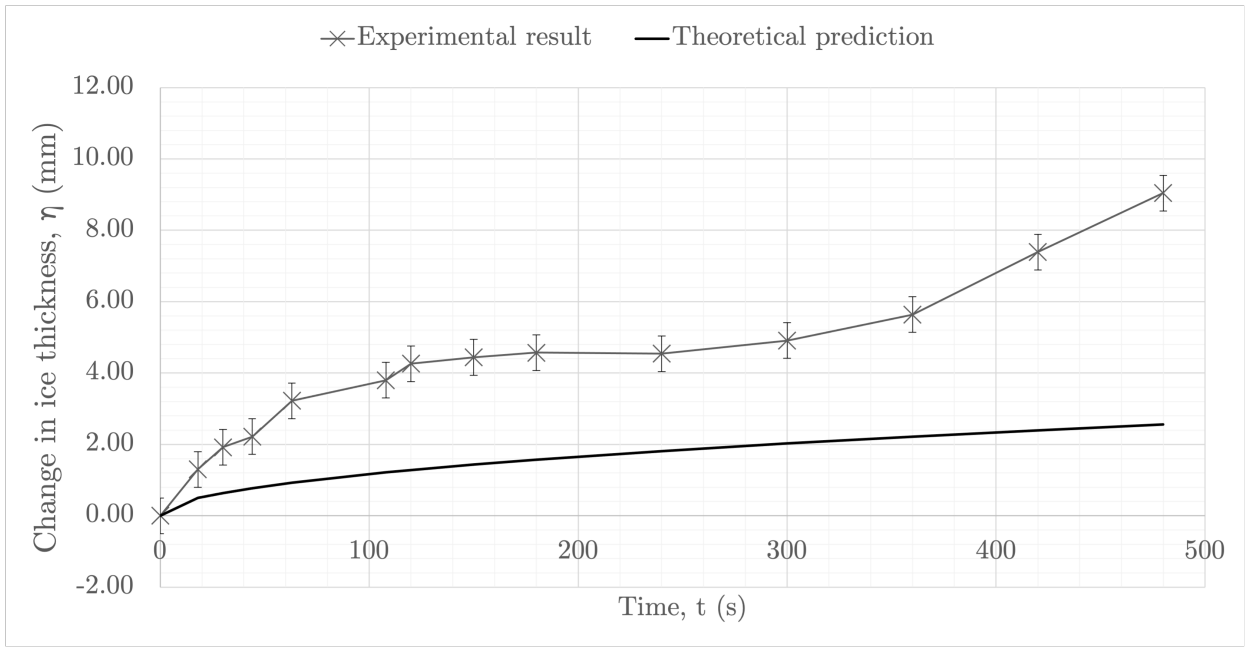

Figure 33: Experiment F: –1.8°C, 32 psu, $x = 0.35$ m. Transient results compared to fresh water theoretical prediction (including moving interface, $T_f = -1.8$°C) with vertical error bars of ±0.5 mm.

termination experiments, the change in ice thickness was averaged across the width of the channel, the transient result gives the change in ice thickness as visible through the Perspex sides (at a singular position across the width). Heat transfer from the water to the sides of the channel means that there is more freezing at the walls, giving an inflated value for change in ice thickness when measured from the photographs. A cross-section of the channel might show the ice forming a U shape due to these contributions. This weakens the quality of the transient results and also invalidates the assumption that behaviour is uniform in the y-direction for water at its freezing temperature. However, the log-log graph of these results

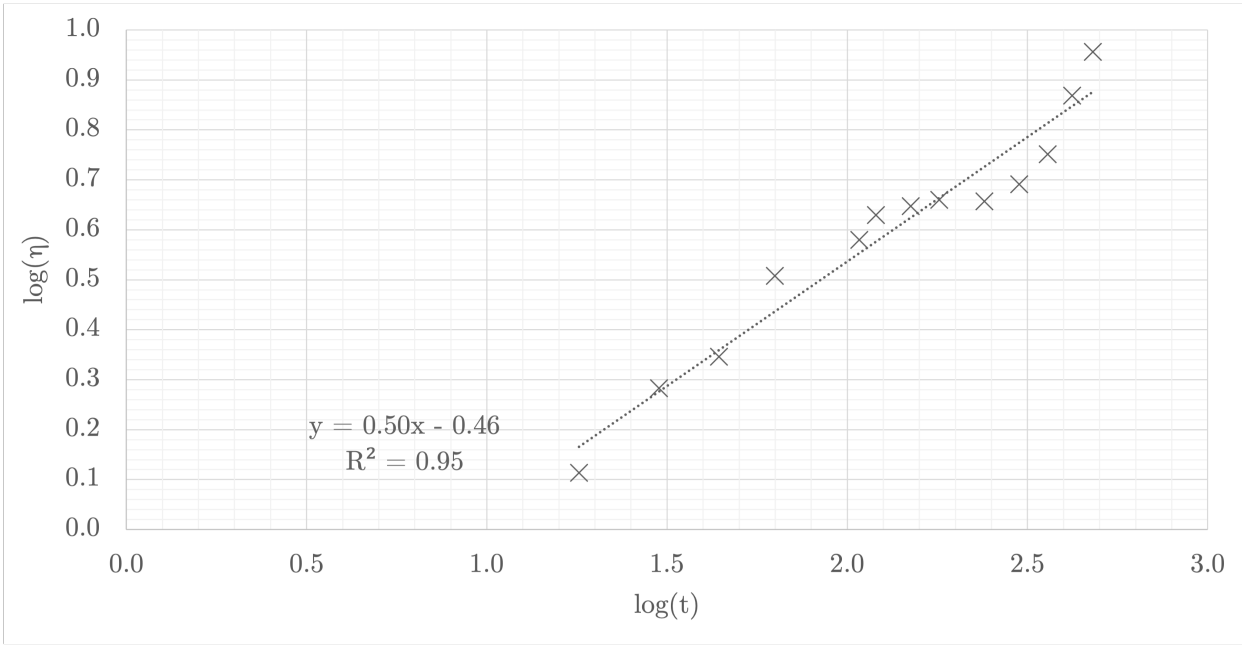

Figure 34: Log-log graph of Experiment F results, with line of best fit $\log \eta = 0.50 \log t - 0.46$ and coefficient of determination R^2=0.95.

(Figure 32) has a line of best fit with gradient 0.45 and an R^2 value of 0.99. This indicates that there is very strong correlation for η having dependence near $\sqrt{t}$. Discrepancies due to heat transfer to the atmosphere, floating ice crystals, and ripples are also likely, as before.

Experiment F (Figure 33) had measurements taken at $x = 0.35$ m, a duration of 6 minutes and used salt water at 32 psu and –1.8°C (its freezing temperature). Again, the transient results significantly exceeded the theoretical prediction and probably for the same reason – conduction to the sides of the channel affecting the local freezing rate and weakening the quality of the results. The log-log graph of Experiment F (Figure 34) has a line of best fit with the expected gradient of 0.5, indicating a $\sqrt{t}$ dependence, but a slightly weaker correlation coefficient of 0.95. This suggests some erratic behaviour, which could be caused by the presence of salt and the mushy layer affecting freezing patterns.

4.3.2 Water initially above its freezing temperature

Experiment G used fresh water at 2°C, had measurements taken at $x = 0.15$ m and a duration of 8 minutes. Figure 35 compares the experimental results with the theoretical prediction for water above the freezing temperature. The model ignoring the boundary layer is used, since it was indicated in Experiment C that, by a distance 0.15 m from the channel inlet, this was more accurate. As predicted, the ice initially thickened and then began to melt after around 50 seconds. Melting began with the newly-formed ice, then after 3 minutes, progressed into the original ice, causing a net loss in ice. This experiment confirmed that the first response of the water is freezing, even when the water is above its freezing temperature (Huppert, 1989 [11]) and the results also validate the theoretical analysis, with the prediction passing through each point's error bar.

In contrast with Experiments E and F, whose results drastically exceeded the prediction, the transient results for Experiment G aligned well. This could be due to the dominant behaviours in the different experiments. In Experiments E and F, which used water at

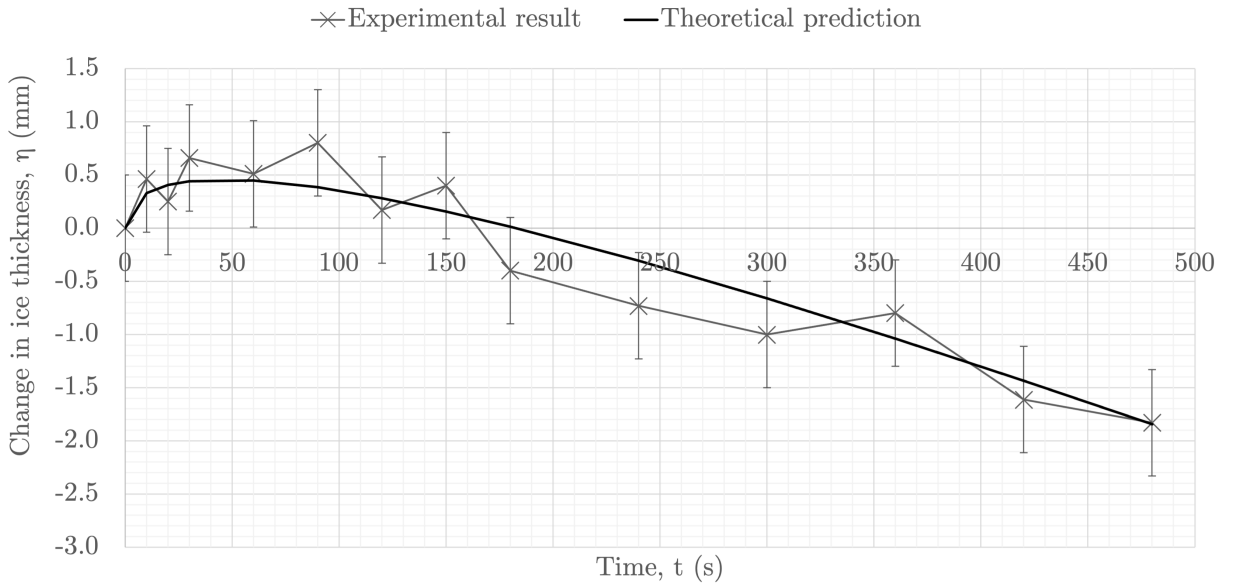

Figure 35: Experiment G: 2°C, fresh water, $x = 0.15$ m. Transient results compared to theoretical prediction (ignoring the boundary layer) with vertical error bars of ±0.5 mm.

its freezing temperature, the only behaviour observed was freezing. In Experiment G, on the other hand, melting was mostly observed. This meant that the undesirable behaviour of conduction from the channel sides was curtailed, since the sides of the channel did not play as significant a role in melting, so changes to ice thickness were more uniform across the channel. In Figure 35, for the first 90 seconds (where freezing occurs) the experimental results look as though they are exceeding the prediction, but as soon as melting is significant, this is no longer a concern.

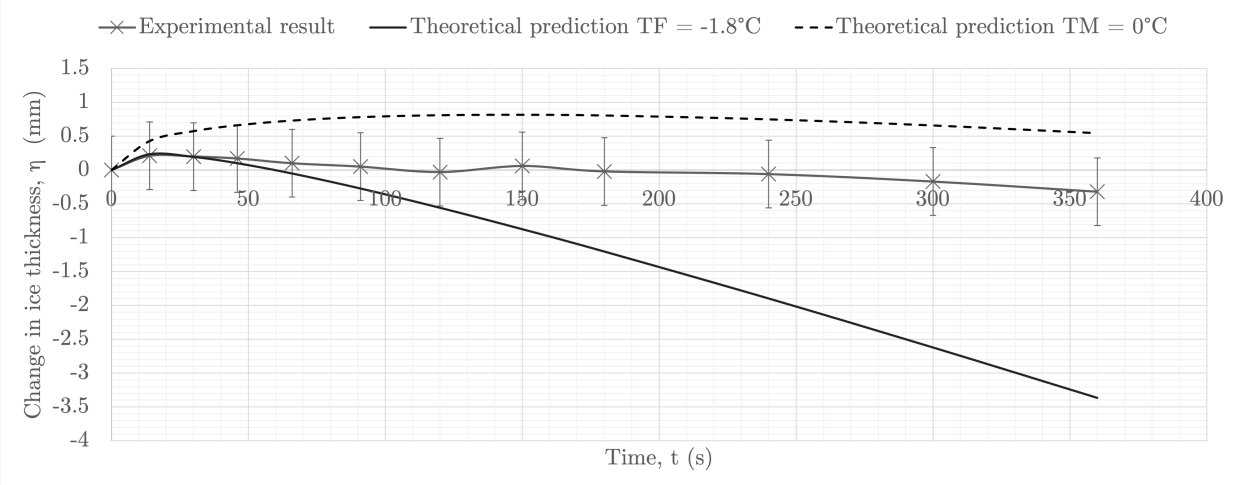

Figure 36: Experiment H: 1°C, 32 psu, $x = 0.15$ m. Transient results compared to two theoretical predictions: $T_f = 0$°C (dashed) and $T_f = -1.8$°C (solid). Both ignoring boundary layer. Vertical error bars of ±0.5 mm.

Experiment H (Figure 36) used salt water at 1°C, had measurements taken at $x = 0.15$ m and a duration of 6 minutes. Two prediction lines are again provided: the lower bound governing freezing of the water (the solid line in Figure 36, with T_f set to –1.8°C in the model) and the upper bound governing melting of the ice (dashed, T_f set to 0°C). The model ignoring the

boundary layer has again been used. As in Figure 30, the experimental results lie between these two lines, suggesting that they are indeed the two governing behaviours and equations. Early in the experiment, for the first minute or so, where freezing is the dominant behaviour, the experimental results almost perfectly match the theoretical prediction governing freezing. Little ice is created, since the water is reasonably far above its freezing temperature and measurements were taken relatively close to the channel inlet, where H_2 is high. However, despite the water being almost 3°C above its freezing temperature, there is also little melting even by the end of the experiment – much less than predicted by the solid line, and much less than was seen in Experiment G, despite the difference between the initial water temperature and the freezing temperature being greater in Experiment H than G. This provides more evidence that the ice grown from salt water has a lower salinity than the water itself, bringing a beneficial effect for the ice volcano, since the water can be above its freezing temperature and still not melt a significant amount of newly-formed or original ice.

4.4 Additional results

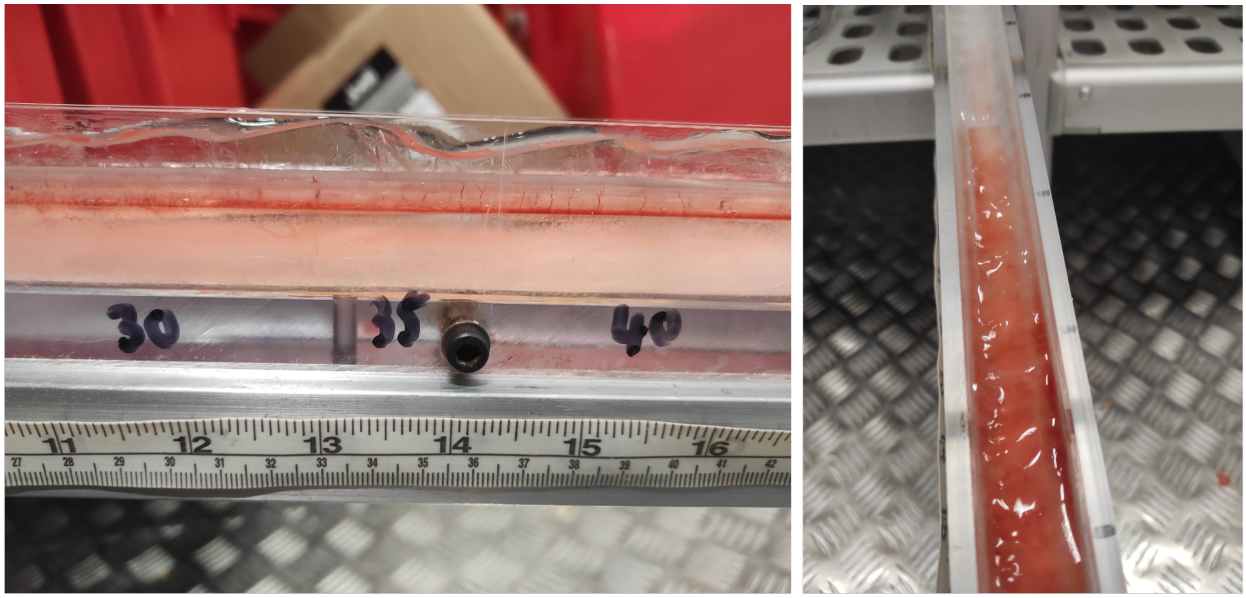

Figure 37: Photographs of ripples in the ice profile after 10 minutes of freezing, in fresh water as seen from the side (left) and in salt water as seen from above (right). Crest-to-trough amplitude is ∼1 cm.

The focus of the experiments was to analyse the ice profile on a large scale – in the termination experiments, measurements were only made every 5 cm along the channel. However, an unexpected result emerged when the profiles were examined closely. Within several minutes, small ripples became visible in the ice. These ripples grew over the course of the experiment, reaching a crest-to-trough amplitude of around 1 cm after 10 minutes (see Figure 37 for examples). Icicles also often exhibit ripples, which are presumed to be due to a morphological instability of ice growth in the presence of a thin flowing water film (Chen and Morris, 2013 [3]). The same process could govern the creation of ripples in these experiments, which also demonstrate ice growth from a thin water film. The growth of the experimental ripples is much faster than that observed in icicles by Chen and Morris, who measured growths of 0.05 cm/hr, though with a much lower flow rate (2.5 ml/min, compared to 5.4 ml/s for these experiments) which may account for the difference. The icicles were also grown vertically, whereas these experiments took place on a shallow 6° slope. Chen and Morris observed that

icicles grown from pure water do not exhibit ripples, yet they were seen in these experiments for both fresh and salt water. However, it was found that even very small levels of dissolved ionic water impurities (as low as 20 mg/l) were sufficient to trigger ripple growth – a condition certainly met by the 'fresh' tap water used in these experiments, with an average $CaCO_3$ content of 281.3 mg/l (Cambridge Water, 2020 [26]). It is unclear whether it is the same physical mechanism driving ripple growth for the icicle as for these experiments, but this would be an interesting area for further research.

The presence of these ripples may have contributed towards discrepancies in the results, particularly for the termination experiments (e.g. if at one position, measurements were taken at the crest of a ripple, and in a trough at the subsequent position), potentially giving an additional uncertainty of ± 5 mm in η after 10 minutes. Nonetheless, for the timescales of these experiments, the ripples did not become large enough to noticeably alter the flow. For longer timescales, it may be worth investigating whether the ripples can become large enough to significantly disrupt the flow and if this could affect the function of an ice volcano.

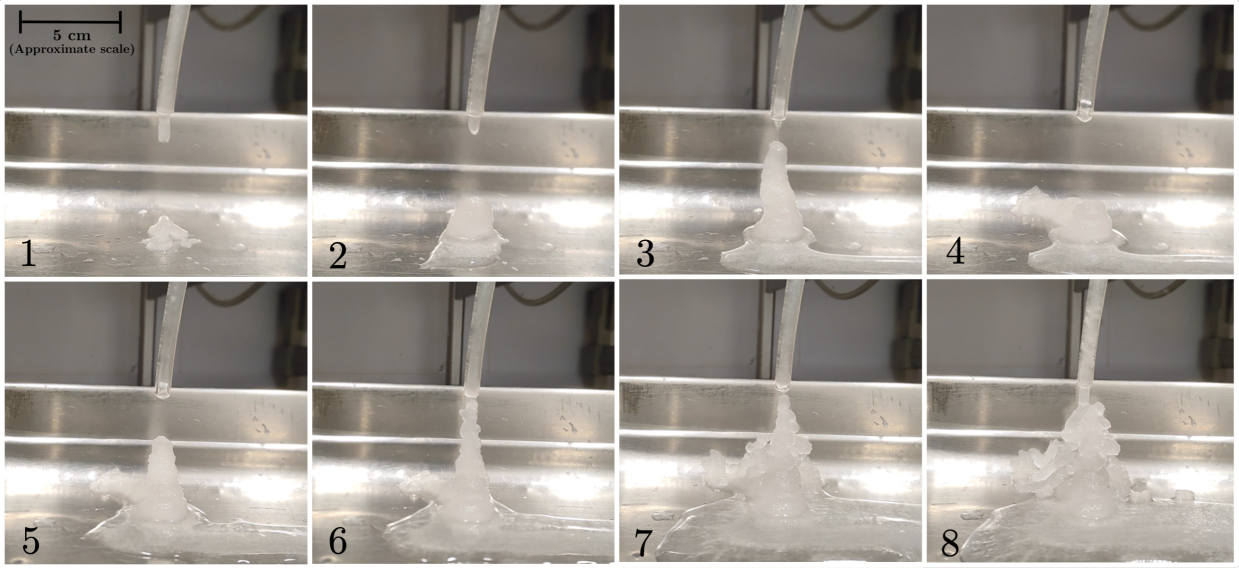

Figure 38: Frames of a video showing cone build-up, using salt water (32 psu) at –1.8°C.

A final exploratory experiment was performed to investigate how the conical shape of an ice volcano might be generated. The water used had a salinity of 32 psu and was at –1.8°C (its freezing temperature). The pump speed was reduced to 15 rpm (with a corresponding flow rate 1.6 ml/s) and a tube positioned over a flat aluminium tray. Slushy ice accumulated directly under the nozzle in a mound, until the mound collapsed under its own weight and became wider and flatter. This process continued and a cone was gradually built up. Figure 38 shows frames from a video of this experiment. This result is promising. Larger-scale and more controlled versions of this experiment would make a good basis from which to develop the ice volcano research.

5 Conclusions and suggestions for further work

The objective of this project was to investigate ice volcanoes as a means to rejuvenate sea ice. A two-dimensional simplified model was established, then evaluated theoretically and experimentally for two fundamental cases: fresh water entering at its freezing temperature and at a warmer temperature. Experiments were conducted using a channel of rectangular cross-section in a walk-in freezer, at a temperature of –18°C. The objective was to assess an ice volcano's feasibility and sensitivity to its environment. Both theoretically and experimentally, the results were promising for water at its freezing temperature: ice formed readily and uniformly all along the channel, indicating an ice volcano could be propitious and homogeneous. Experimental ice build-up exceeded theoretical predictions for both fresh and salt water, potentially due to heat fluxes from the air that were neglected in the model. However, results were less encouraging for water entering the channel above its freezing temperature. It was found that this results in a substantial loss of ice near the inlet even for water just a few degrees above its freezing temperature, although ice is still created further down the channel. In the context of the ice volcano, this insinuates that the region of ice surrounding the pipe could be completely eroded within a few hours, creating an 'ice doughnut', unless the water is within a very narrow margin of its freezing temperature. This narrow range for acceptable water temperature poses operability issues. At certain temperatures, an ice volcano could even melt more ice than it creates, making it entirely unfeasible and counterproductive.

The experimental analysis was also extended to salt water, which had some notable differences. Firstly, the 'ice' grown from salt water was in fact a two-phase mixture of pure ice and concentrated brine, with a melting temperature higher than the freezing temperature of the salt water itself. This has a beneficial effect for the ice volcano, because if the ice melts at a warmer temperature than the water freezes, the water may be above its freezing temperature and still not melt the ice, increasing the range of operable temperatures. When salt water was used experimentally, the ice loss at the channel inlet was less than half of that observed for fresh water (for water temperatures equivalently above their respective freezing temperatures). However, if the salt water were warm enough, it would still cause the disastrous ice losses described above and render the ice volcano ineffective.

Some implications for the design of an ice volcano have arisen during this project:

- It must prevent ice loss around the pipe of the manner described above. Solutions could include: switching off the ice volcano when the sea temperature is above a preset value; periodically pausing the flow and allowing any holes to be filled up; eliminating the slotted pipe and forcing the water to flow vertically down over the whole pipe, so that it is at the freezing temperature by the time it reaches the ice.
- It should provide a means for brine to drain out of the newly-formed ice, so that the ice is strengthened and has a higher melting temperature.

An interesting theoretical result, though not of direct relevance to the ice volcano, is that when water comes into contact with cold ice, the first response is always for the water to freeze. This occurs regardless of the original temperature of the water and at an initially infinite rate. Subsequently, the rate of freezing slows, followed by melting for water above its freezing temperature. This was also demonstrated experimentally in Section 4.3.2.

Recommendations for further work on this topic include:

- Developing the theoretical model for a three-dimensional cone and for salt water.
- Improving the accuracy of the model over long timescales, by accounting for convection, radiation and evaporation from the water to the atmosphere and removing the semi-infinite ice assumption.
- Investigating ripple and/or rivulet formation in detail and determining their impact on ice build-up.
- Continuing the experimental analysis with salt water, ideally using a cone and over longer timescales. Testing the salinity of the resulting ice/brine mixture would also be extremely valuable to understand the underlying processes governing ice formation.
- Beginning detailed design for an ice volcano, and then building and testing a prototype in Arctic conditions.
- Considering the magnitude and source of the power requirements for an ice volcano.
- Exploring feasible sea and air temperatures for ice volcanoes and linking this to Arctic weather patterns, to suggest how, where and when they might be implemented.

Acknowledgements

I am extremely grateful to my supervisors, Dr Shaun Fitzgerald and Professor Hugh Hunt, Department of Engineering, University of Cambridge, for their invaluable support and feedback throughout this project. Likewise, this project would not have been possible with the generosity and patience of Ian Reinhardt and all staff in the kitchens of Trinity College, Cambridge, who allowed me to use their freezer for over three months to conduct my never-ending experiments. I am also indebted to Dr Lotty Gladstone, from the BP Institute, for lending me the pump; and to Stefan Savage, from the Department of Engineering, University of Cambridge, for constructing the ice channels used in my experiments.

I would also like to thank Professor Grae Worster, Department of Applied Mathematics and Theoretical Physics, University of Cambridge; Professor Herbert Huppert, Institute of Theoretical Geophysics, University of Cambridge; and Professor Peter Wadhams, Department of Applied Mathematics and Theoretical Physics, University of Cambridge; for their guidance and expertise in fluid dynamics, heat transfer, and the mechanics of sea ice.

References

[1] Steven Amstrup, Bruce Marcot, and David Douglas. A Bayesian Network Modeling Approach to Forecasting the 21st Century Worldwide Status of Polar Bears. *Geophysical Monograph Series, American Geophysical Union, Washington DC*, 180:213–268, 2008.

[2] C. M. Bitz and William H. Lipscomb. An energy-conserving thermodynamic model of sea ice. *Journal of Geophysical Research: Oceans*, 104(C7):15669–15677, 1999.

[3] Antony Szu-Han Chen and Stephen W Morris. On the origin and evolution of icicle ripples. *New Journal of Physics*, 15, 2013.

[4] William S. Clarke. *Proposals for a consortium to implement Climate Restoration*, 2016. Available from: http://www.2greenenergy.com/wp-content/uploads/2016/03/Climate-Restorationv4d.pdf [Last accessed 23/05/22].

[5] J. C. Comiso. Large decadal decline of the arctic multiyear ice cover. *J. Clim.*, 25(4):1176–1193, 2012.

[6] Adam Corner and Nick Pidgeon. Geoengineering the climate: The social and ethical implications. *Environment: Science and Policy for Sustainable Development*, 52(1):24–37, 2010.

[7] S.J. Desch et al. Arctic ice management. *Earth's future*, 5:107—-127, 2017.

[8] D. Feltham, N Untersteiner, J. Wettlaufer, and M. Worster. Sea ice is a mushy layer. *Geophys. Res. Lett*, 33, 2006.

[9] L. Field et al. Increasing arctic sea ice albedo using localized reversible geoengineering. *Earth's Future*, 6(6):882–901, 2018.

[10] Nicolas Gruber, Charles Keeling, and Nicholas Bates. Interannual variability in the north atlantic ocean carbon sink. *Science*, 298(5602):2374–2378, 2002.

[11] Herbert Huppert. Phase changes following the initiation of a hot turbulent flow over a cold solid surface. *Journal of Fluid Mechanics*, 198:293–319, 1989.

[12] Lee R. Kump, Alexander Pavlov, and Michael A. Arthur. Massive release of hydrogen sulfide to the surface ocean and atmosphere during intervals of oceanic anoxia. *Geology*, 33(5):397–400, 2005.

[13] Zachary Labe. *Arctic Temperatures*, 2022. Available from: https://sites.uci.edu/zlabe/arctic-temperatures/ [Last accessed 30/05/22].

[14] Nan Li et al. Heat transfer at ice-water interface under conditions of low flow velocities. *Journal of Hydrodynamics*, 28(4):603–609, 2016.

[15] L. Miller et al. *Implications of Sea Ice Management for Arctic Biogeochemistry*, 2020. Available from: https://eos.org/opinions/implications-of-sea-ice-management-for-arctic-biogeochemistry [Last accessed 22/05/22].

[16] D. A. Rothrock, Y. Yu, and G. A. Maykut. Thinning of the arctic sea-ice cover. *Geophysical Research Letters*, 26(23):3469–3472, 1999.

[17] Axel Schweiger et al. Uncertainty in modeled arctic sea ice volume. *Journal of Geophysical Research: Oceans*, 116(C8), 2011.

[18] Natalia Shakova, Igor Semiletov, et al. Extensive methane venting to the atmosphere from sediments of the east siberian arctic shelf. *Science*, 327(5970):1246–1250, 2010.

[19] National Snow and Ice Data Center. *Salinity and Brine*, 2020. Available from: https://nsidc.org/cryosphere/seaice/characteristics/brine_salinity.html [Last accessed 26/05/22].

[20] Benjamin Sovacool. Reckless or righteous? reviewing the sociotechnical benefits and risks of climate change geoengineering. *Energy Strategy Reviews*, 35:100656, 2021.

[21] Florian Sévellec, Alexey V. Fedorov, and Wei Liu. Arctic sea-ice decline weakens the atlantic meridional overturning circulation. *Nature Climate Change*, 7(8):604–610, 2017.

[22] G. D. Towell and L. B. Rothfeld. Hydrodynamics of rivulet flow. *AIChE Journal*, 12:972–980, 1966.

[23] Harvard University. *Science and cooking lecture series 2021*, 2021. Available from: https://sciencecooking.seas.harvard.edu/ [Last accessed 22/05/22].

[24] Peter Wadhams. *Ice in the Ocean*. Gordon and Breach Science Publishers, London, 2000.

[25] Peter Wadhams. *A Farewell to Ice: A Report from the Arctic*. Penguin Books, London, 2017.

[26] Cambridge Water. *Cambridge City North water quality zone (Z1)*, 2020. Available from: https://www.cambridge-water.co.uk/household/my-water-supply/water-quality/water-quality-standards/cambridge-city-north-water-quality-zone-z1 [Last accessed 17/05/22].

[27] Megan D. Willis, W. Richard Leaitch, and Jonathan P.D. Abbatt. Processes controlling the composition and abundance of arctic aerosol. *Reviews of Geophysics*, 56(4):621–671, 2018.

A Risk assessment retrospective

A risk assessment was submitted at the beginning of the project. Three main experimental hazards were identified: the use of salt water, which may cause vomiting if ingested; the heavy channels, which could cause a foot injury if dropped; and the –18°C freezer, which posed numerous risks. In retrospect, the risk assessment was complete, thorough, and accurately reflected the hazards encountered during the experiments (though perhaps overestimating their likelihood). Throughout the project, risks were well-managed and no incidents occurred. The Trinity College kitchen staff, who checked on me every 15 minutes whilst I was using the freezer, comprised the most critical risk management strategy, since this mitigated the most severe danger (hypothermia). If I were to repeat the project, I would not assess risk any differently, as the experiments ran successfully and safely. The chosen form of risk assessment (a risk matrix) clearly illustrated the hazards and the likelihood and severity of their associated risks, and proposed suitable and effective risk management strategies.